Marine Chemistry
January 2024, Volume 258, Pages 104347 (12p.)
https://doi.org/10.1016/j.marchem.2023.104347 https://archimer.ifremer.fr/doc/00867/97893/

Tracing anthropogenic aerosol trace metal sources in the North Atlantic Ocean using Pb, Zn and Ni isotopes

Zhang Xingchao [1, 2, *], Lemaitre Nolwenn [1, 3], Rickli Jörg Dominik [1], Suhrhoff Tim Jesper [1], Shelley Rachel [4, 5], Benhra Ali [6], Faye Saliou [7], Jeyid Mohamed Ahmed [8], Vance Derek [1]

[1] Institute of Geochemistry and Petrology, Department of Earth Sciences, ETH Zürich, Clausiusstrasse 25, Zürich 8092, Switzerland
[2] CAS Key Laboratory of Crust-Mantle Materials and Environments, School of Earth and Space Sciences, University of Science and Technology of China, Hefei 230026, China
[3] LEGOS, Université de Toulouse, CNRS, CNES, IRD, UPS, Toulouse, France
[4] Univ Brest, CNRS, IRD, Ifremer, LEMAR, Plouzane F-29280, France
[5] School of Environmental Science, University of East Anglia, Norwich NR4 7TJ, UK
[6] Laboratoire d'Ecotoxicologie, Institut National de Recherche Halieutique (INRH), 2, rue Tiznit, Casablanca, Morocco
[7] Laboratoire d'Ecotoxicologie, Institut National de Recherche Halieutique (INRH), 2, rue Tiznit, Casablanca, Morocco
[8] Institut Mauritanien de Recherches Océanographiques et des Pêches (IMROP), Nouadhibou BP 22, Mauritania

* Corresponding author : Xingchao Zhang, email address : Zhangxc@mail.ustc.edu.cn

Abstract :

Atmospheric deposition of trace metals of natural or anthropogenic origin is an important input of micronutrients to the surface ocean. However, understanding its direct impact on oceanic element cycles is challenging due to scarce data, coupled to diverse aerosol sources and variable solubilities. Here, we present a dataset that combines Ni, Zn and Pb isotopes for samples from the Moroccan and Senegalese coasts and in the high latitude North Atlantic Ocean. We combine the new with published data for other circum-North Atlantic sources to assess the processes that determine the isotope signatures in different types of aerosols. We then use open marine aerosol data to investigate the impact of these signatures in the open ocean. Isotope analyses were conducted on bulk aerosols (>20 µm), on their ultra-high-purity water leachates, and on rainwaters. Aerosols characterized by crustal elemental abundances have isotope compositions similar to Saharan mineral dust. Mixing with anthropogenic aerosols from Europe/North Africa results in lower 206Pb/207Pb and 208Pb/207Pb values for the Eastern North Atlantic region. Higher 206Pb/207Pb at a given 208Pb/207Pb, observed near the Canadian margin and occasionally at the Senegalese coast, points to anthropogenic inputs from North America. Based on trends in the aerosol data (e.g., δ66ZnJMC-Lyon versus 206Pb/207Pb, δ60NiSRM986 versus Ni/V), we identify several anthropogenic sources of Zn and Ni. The δ66ZnJMC-Lyon of low-temperature pollution (e.g., non-exhaust traffic emission) appears to be around −0.1‰ to 0.2‰, while leachate δ66ZnJMC-Lyon as low as −0.21‰ indicates contributions from high-temperature combustion or smelting processes. Among aerosols with good correlations between Ni and V, δ60NiSRM986 > 0.40‰ traces Ni contributions from oil combustion. Other Ni-enriched sources, possibly originating from laterite or sulfide, show relatively

low δ60NiSRM986 (as low as −0.85‰) and low V/Ni. Generally, aerosol sources for Zn are consistent throughout the North Atlantic, while Ni can be highly heterogenous. Combining the new data with literature elemental data, ratios of soluble Zn/Pb in anthropogenic aerosols are 1–100 times surface ocean ratios, suggesting that the low δ66ZnJMC-Lyon observed in anthropogenic aerosol can be key in controlling the upper ocean Zn isotope composition. These aerosols have, however, much less significance for surface ocean Ni.

Graphical abstract

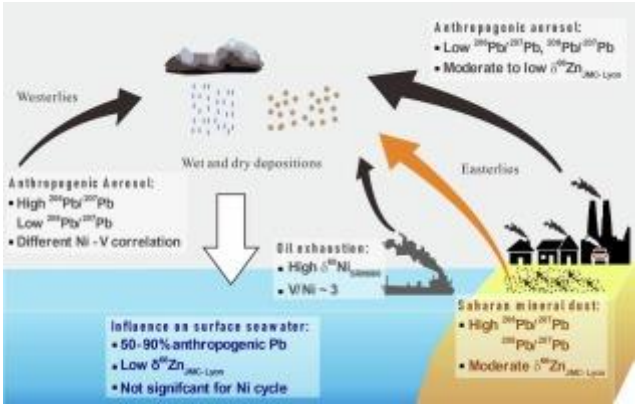

Highlights

► Impacts from Saharan dust, and high-T and low-T anthropogenic emissions can be identified with Zn-Pb and Zn isotopes; ► Nickel isotopes indicate contributions from oil combustion and lithogenic particles; ► Anthropogenically sourced aerosol may be a key factor in determining the low $\delta^{66}Zn$ in surface seawater; ► These aerosols may be less significant for surface ocean Ni.

Keywords : Ni, Pb, Zn isotopes, aerosol sources, surface ocean, North Atlantic Ocean.

1. Introduction

Trace metals (TMs), including nickel and zinc (Ni and Zn), are essential micronutrients for marine phytoplankton because of their requirement by metalloenzymes (Sunda, 1988; Morel and Price, 2003). An important source of these TMs to the ocean is via dry (aerosol: dust, soil, ash) and wet (precipitation: rain, fog, snow) atmospheric deposition (e.g., Hamilton et al., 2022). Natural mineral dust is one of the main components of atmospheric aerosols (Jickels et al., 2005), but it is relatively insoluble in seawater (Mahowald et al., 2018). In contrast, though anthropogenic activities and natural pyrogenic processes (e.g., wildfire) produce less aerosol, their trace metal inventory is more soluble, so that they may supply proportionally more bioavailable TMs to the surface ocean (e.g., Ito et al., 2019; Hamilton et al., 2022; König et al., 2022). Therefore, disentangling the atmospheric TM sources of different natural and anthropogenic origins is important to better quantify the soluble (and bioavailable) fraction of TMs deposited from atmosphere into the surface ocean, and to improve our understanding of their anthropogenically influenced biogeochemical cycling.

The Ni and Zn stable isotope compositions ($\delta^{60}Ni_{SRM986}$ and $\delta^{66}Zn_{JMC\text{-}Lyon}$ = variations in $^{60}Ni/^{58}Ni$ and $^{66}Zn/^{64}Zn$ ratios expressed as parts per thousand deviations from the NIST SRM 986 and JMC Lyon standards, respectively) are powerful in discriminating different sources and processes at play in the ocean. A shift towards light Zn isotope signatures in the dissolved pool is observed within the upper ocean, north of the Southern Ocean (e.g., Conway and John, 2014; John et al., 2018; Lemaitre et al., 2020a). Debate continues concerning the origin of this light Zn isotope signal, which could be due either to scavenging removal of heavy isotopes (John and Conway, 2014; Weber et al., 2018) or to external input of a light isotope signature (Lemaitre et al., 2020a; Liao et al., 2020, 2021). A better constraint on the $\delta^{66}Zn_{JMC\text{-}Lyon}$ signatures of atmospheric depositions is required to resolve this problem. The $\delta^{60}Ni_{SRM986}$ distribution in the surface ocean is mainly controlled by biological uptake along with water mass mixing (e.g., Archer et al., 2020; Yang et al., 2021; Lemaitre et al., 2022). However, the potential impact from atmosphere deposition on

surface Ni cycling is not quantified due to a lack of aerosol data.

Distinctly low $\delta^{66}Zn_{JMC\text{-}Lyon}$ values (as low as -0.73‰) are produced in controlled industrial emissions (Mattielli et al., 2009) compared to mineral dust (average of 0.24‰; Dong et al., 2013; Schleicher et al., 2020; Zhang et al., 2022), while coal and biomass burning produce aerosols with much higher $\delta^{66}Zn_{Lyon}$ (up to 0.8‰; Schleicher and Weiss, 2023). Low $\delta^{66}Zn_{JMC\text{-}Lyon}$ is observed for marine aerosols (Dong et al., 2013; Little et al., 2014; Liao et al., 2020, 2021; Packman et al., 2022) and, interestingly, is found in seawater and in marine particles (Lemaitre et al., 2020a; Liao et al., 2020, 2021). The $\delta^{60}Ni_{SRM986}$ of crude oil (0.42 to 0.75‰; Ventura et al., 2015), one of the most important anthropogenic Ni sources to the atmosphere, is distinctly higher than most lithogenic materials, such as rocks and soils (-0.33‰ to 0.32‰; Gueguen et al., 2013; Gall et al., 2017; Ratié et al., 2015), laterite ores (-0.61‰ to 0.32‰; Ratié et al., 2016, 2018) and magmatic sulfides (-1.04‰ to -0.10‰; Hofmann et al., 2014). Mixing between oil combustion-derived and lithogenic Ni has been suggested to explain the $\delta^{60}Ni_{SRM986}$ range (0.05‰ to 0.56‰) of aerosols in the South China Sea (Takano et al., 2020).

All of the above information comes from very few studies: aerosol data are still very scarce for Zn and almost non-existent for Ni. Thus, although different 'endmembers' have been defined in terms of their Zn and Ni isotope composition, challenges remain in identifying the impact from specific sources on dissolved surface ocean inventories, especially in regions with multiple aerosol sources such as the North Atlantic. In this ocean basin, lead (Pb) has been used to study anthropogenic inputs more than in any other (e.g., Boyle et al., 2014). Anthropogenic inputs of Pb from North America and Europe/Africa show distinct isotope ratios ($^{206}Pb/^{207}Pb$ and $^{208}Pb/^{207}Pb$) compared to natural inputs from the Saharan desert (e.g., Komárek et al., 2008; Boyle et al., 2014; Bridgestock et al., 2016, 2018). Combining Pb with Ni and Zn isotope analyses, and further elemental ratios, will therefore help in constraining the origin of Ni and Zn in aerosols and ocean waters.

Here we present data for the Ni, Zn and Pb isotope compositions in bulk aerosols (>20 μm), gentle leachates, and in rainwaters, all collected off the Moroccan (EPURE)

and Senegalese (AWA) coasts and in the higher latitude open North Atlantic Ocean (GEOVIDE). Though the coastal samples (AWA and EPURE) are geographically restricted, they are representative of some key processes that define source isotope signatures, and, including Pb isotope data, provide a near source characterization of the aerosol end-members that can be transported into the oceanic region. We also compile published constraints on the isotope compositions of aerosols from other sources around the North Atlantic. The new and compiled data were then compared with those from GEOVIDE, as well as previous data from the equatorial and eastern Atlantic, to better understand the compositional variations in the atmosphere throughout the North Atlantic. Finally, the isotope compositions of the soluble fractions were compared with surface seawater to understand how atmospheric deposition affects the surface ocean.

2. Material and methods

2.1. Study areas and sample collection

The aerosol (>20 μm) and rainwaters were collected from three different regions. Two sets were collected close to the Sahara Desert and surrounding cities, representing both natural and anthropogenic dust sources (AWA and EPURE), whereas a third was collected in the open high-latitude North Atlantic (GEOVIDE) (Fig. 1; Tables S1, S2, S3).

The GEOVIDE cruise (GEOTRACES section GA01; 15 May-30 June 2014, R/V *Pourquoi Pas?)* departed from Lisbon (Portugal), sailed to the Greenland shelf, and ended in St John's (Newfoundland, Canada; Fig. 1a). Station records, satellite imagery, positive matrix factorization and air mass back trajectory simulations suggest a mixture of airborne particles (i.e., aerosol from Africa, Europe, North America, Iceland and sea salt), affected by seasonal cycles and higher pollutant contributions closer to the European and North American continents (Prospero et al., 2012; Shelley et al., 2017, 2018). Both wet (precipitation) and dry (aerosol) deposition samples were collected, with sampling details given in Shelley et al. (2017). In brief, for aerosol samples, air was pulled through 47 mm diameter Whatman 41 (W41, 20 μm pore size)

ashless filter discs at approximately 1.2 m^3/min (134 cm/s face velocity) using a high-volume aerosol sampler (~1 m^3/min; model TE 5171, Tisch Environmental). To avoid contamination from sea spray and the ship's exhaust stack, aerosol samplers were placed on the ship's flying bridge and were sector (± 60° from the bow) and wind speed (> 0.9 m/s) controlled, using an anemometer and a vane attached to a 3m pole mounted on the railings near the aerosol sampler. The aerosol filters were frozen directly after collection and stored at -20°C. Precipitation samples (rainwaters) were collected on an event basis using a Teflon precipitation sampler, and rainwaters were acidified onboard to 0.024 M HCl (Ultrapur, Merck). The relatively low Al loadings (1 to 30 ng per m^3 of air) in GEOVIDE aerosols suggests limited influence from the Sahara at the time of sampling, and wet deposition accounts for an important part of the total (wet + dry) TM deposition (Shelley et al., 2017).

The AWA project (Fig. 1c, d) consisted of three different cruises off the Senegalese coast: UPSEN-2 (AWA-U), ECOAO (AWA-E) took place in spring 2013 (23 February- 2 March and 7-19 March; Fig. 1c; R/V *Antea*); AWA (AWA-A) in spring 2014 (4-14 March, Fig. 1d; R/V *Thalassa*). Aerosols from this area are thought to be composed of a mixture of Saharan mineral dust and urban pollutants (Petzold et al., 2011). Naidja et al. (2018) have also suggested that soil dust, biomass burning, diesel-powered vehicles and industrial activities can be important sources of atmospheric particles in Africa, and may hence be important sources of TMs in aerosols collected during the AWA project. Similar sampling approaches as described above for GEOVIDE have been used to collect dry deposition samples. The aerosol optical depth data (AOD data; http://aeronet.gsfc.nasa.gov) suggest higher dust loadings during sampling periods in 2014 than in 2013 (Fig. 1c and 1d), but no significant differences were observed in atmospheric Al loadings between UPSEN-2/ ECOAO (200 to 6000 ng/m^3) and AWA (70 to 4000 ng/m^3) cruises (Table S1).

The EPURE project sampled aerosols 100 – 800 m inland from the Moroccan coast, up wind of Agadir and Dakhla (Fig. 1e). The Agadir site (EPURE-Ag) is located close to an important industrial area, including crude oil refineries, phosphate-based fertilizer manufacturing and power plants (Rodriguez et al., 2011). In

contrast, the Dakhla site (EPURE-Dak) is located further south and generally displays greatest aerosol contributions from mineral dusts (Shelley et al., 2016). Samples were collected from March 2015 to March 2016 using a low-volume sampler manufactured in-house. Wind speed (> 0.9 m/s) and sector were monitored to minimize the sampling of local emissions. The high Al loadings (15 to 6000 ng/m^3) observed during EPURE suggest significant impact of the Saharan dust plume (Shelley et al., 2016).

2.2. Sample processing and elemental analyses

Elemental contents of bulk aerosol samples, their ultra-high-purity (UHP, 18.2 MΩ/cm resistivity, pH~5.5) water leachates, and rainwater were obtained at LEMAR (France) and have been discussed in detail in previous publications (Shelley et al., 2016, 2017, 2018). The new isotope analyses in this study were performed at ETH Zurich on aliquots of sample stock solutions, as summarized below.

As detailed in Shelley et al. (2016, 2017), the W41 filter discs were digested for bulk aerosol analyses in a 5:1 mixture of concentrated HNO_3 and HF (v/v, ~14 M and ~24 M, respectively, Ultrapur, Merck), refluxing at 150°C. After evaporation, concentrated HNO_3 was added to break down fluoride salts. The residues were then dissolved in 0.4 M HNO_3. For UHP water leaching experiments, 100 mL of UHP water was rapidly passed through an aerosol-covered W41 filter disc, placed above a GN-6 Metrical backing filter (cellulose esters, ≤ 0.45 µm). The leachate was then acidified to 0.024 M (pH~1.7) with HCl (Ultrapur, Merck). Rainwater samples were shaken vigorously, and approximately 2 ml of sample was pipetted, evaporated and dissolved in 0.4 M HNO_3. These solutions were analyzed by high-resolution-inductively coupled plasma mass spectrometry (HR-ICP-MS; Element 2, Thermo-Fisher). A 1 ppb indium solution was used as internal standard for drift correction. Details of the analyses of blanks and certified reference materials (including a dust reference material LKSD-1) are reported in Table S1 of Shelley et al. (2017). The elemental contents of bulk aerosols were converted into elemental concentrations per volume of air (atmospheric loadings, e.g. ng element per m^3 of air) using the respective sampled air volumes.

For the purposes of this study (i.e., the analysis of Pb, Zn and Ni isotopes), elemental concentrations of the chosen solutions, including bulk aerosol digests from AWA and EPURE, water leachates from AWA and GEOVIDE, and rainwater from GEOVIDE, were re-measured by HR-ICP-MS (Element XR, Thermo-Fisher) at ETH Zurich. Similar elemental ratios were determined, suggesting no significant changes during storage (Tables S1, S2 and S3). Furthermore, Na was also analyzed to trace the potential impact of sea salt (e.g., Marsay et al., 2022). The potential contribution of sea salt to observed Pb, Zn and Ni amounts is less than 0.01% and is thus ignored here (Table S1). The enrichment factor (EF) compared to crustal elemental abundances was determined as:

$$EF = ([Element] / [Al])_{Aerosol} / ([Elements] / [Al])_{UCC} \quad \text{(Eq. 1)}$$

where the upper continental crust (UCC) concentrations are from Rudnick and Gao (2014). The molar ratios of V/Ni were also calculated (see Tables S1-3). Turnover times with respect to atmospheric deposition are calculated for both the western and eastern sections of the GEOVIDE transect (boundary at 30°W, as suggested in Shelley et al., 2017):

$$\text{Turnover time} = [Zn]_{mixed\ layer} \times [Depth]_{mixed\ layer} / [Flux]_{total} \quad \text{(Eq.2)}$$

Turnover time is defined as the integrated dissolved Zn concentration in the mixed layer (Lemaitre et al., 2020a) divided by the total soluble Zn deposition flux (leachate + rainwater samples; Shelley et al., 2017, 2018).

2.3. Isotope analyses

For Zn and Ni isotopes, a distinction was made between samples characterized by Zn/Ni concentration ratios between 0.25 and 4, and by Zn/Ni ratios >4 or <0.25. This is because a narrow range of sample/spike ratios is required in analyte solutions. For samples with Zn/Ni concentration ratios between 0.25 and 4, ^{64}Zn-^{67}Zn and

^{61}Ni-^{62}Ni double spikes were added to the same aliquot to yield sample/spike elemental ratios of 0.5-2. After a 48-h equilibration period, the solutions were first passed through an anion exchange column (AGMP-1 resin, Bio-Rad), separating Zn from Ni and most of the matrix (Archer et al., 2004; Vance et al., 2016; Wang et al., 2019). Zinc was further purified on a second identical column. The impure Ni-matrix fractions were passed through a Nobias-chelate PA1 resin bed (Hitachi High Technologies) to remove matrix cations, principally Na, Mg and Ca (Wang et al., 2019; Archer et al., 2020), followed by a AG50W-X8 resin (Bio-Rad) and Re resin (Eichrom) columns to remove residual Fe, Al, and Ti (Little et al., 2020). A final Nobias column was performed to guarantee complete purification of Ni fractions (Little et al., 2020; Sun et al., 2021). The same procedure, but with separate sample aliquots for Zn and Ni was applied for samples with Zn/Ni concentration ratios >4 or <0.25. The blanks of the chemical procedures are less than 2 ng for Zn and 0.5 ng for Ni, compared to sample sizes of ~100 ng for Zn and 20 to 50 ng for Ni. Reported isotope ratios were not corrected for these small blank contributions (< 2% for Zn, < 2.5% for Ni).

For Pb isotope analysis, separate aliquots were evaporated and re-dissolved in 1M HBr. This step was repeated three times before isolating Pb on an anion exchange column (AG1-X8 resin, Bio-Rad) using mixed HBr-HNO_3 solutions (Lugmair and Galer, 1992). The total blank of this chemical procedure is less than 20 pg for Pb, compared to sample quantities of ~10 ng. Reported Pb isotope ratios were also not corrected for these minor blank contributions < 0.2 %.

The pure Pb, Ni and Zn fractions were analyzed for their isotope ratios using a Thermo-Finnigan Neptune Plus multi-collector inductively-coupled-plasma mass spectrometer (MC-ICP-MS) in low resolution mode at ETH Zurich. Samples were dissolved in 0.5-1 ml 0.3 M HNO_3 and introduced via a Savillex C-Flow PFA nebulizer (50 µl/min) attached to an Aridus II desolvator. For Zn and Ni, double spike methods were used to correct for instrumental mass bias and any isotope fractionation induced during column chemistry (Bermin et al., 2006; Cameron et al., 2009, 2014). For Zn analysis, ^{62}Ni and mass 68.5 were monitored to correct minute interferences

from ^{64}Ni on ^{64}Zn and from doubly charged Ba. The primary ETH-AA Zn standard was used during Zn isotope measurements, and the results are reported relative to the JMC-Lyon standard based on a well constrained δ^{66}Zn difference between the two standards of 0.28‰ (Archer et al., 2017) as follows:

$$\delta^{66}Zn_{JMC\text{-}Lyon} = [(^{66}Zn / ^{64}Zn)_{sample} / (^{66}Zn / ^{64}Zn)_{ETH\text{-}AA} - 1] \times 1000 + 0.28 \text{ (‰)} \quad \text{(Eq. 3)}$$

The long-term reproducibility of Zn isotope analysis was assessed based on seven years of repeat analyses of the secondary IRMM-3702 standard, which yields $\delta^{66}Zn_{JMC\text{-}Lyon}$ = 0.30 ± 0.06‰ (2SD; n = 795). This is identical to values previously published: $\delta^{66}Zn_{Lyon}$ = 0.28 ± 0.02 ‰ (Archer et al., 2017).

For Ni, ^{56}Fe and ^{57}Fe were measured to correct minute interferences from ^{58}Fe on ^{58}Ni. Nickel isotope compositions are reported in delta notation relative to the primary NIST SRM 986 standard as follows:

$$\delta^{60}Ni_{SRM986} = [(^{60}Ni / ^{58}Ni)_{sample} / (^{60}Ni / ^{58}Ni)_{NIST\ SRM\ 986} - 1] \times 1000 \text{ (‰)} \quad \text{(Eq. 4)}$$

The long-term reproducibility for Ni isotope analysis was monitored by repeat analyses of the secondary standards NOD A1 ($\delta^{60}Ni_{SRM986}$ = 1.04 ± 0.08 ‰; 2SD; n = 372) and NOD P1 ($\delta^{60}Ni_{SRM986}$ = 0.34 ± 0.08‰; 2SD; n = 440). The obtained isotope compositions are consistent with the literature: $\delta^{60}Ni_{SRM986}$ = +1.03 ± 0.06 ‰ for NOD A1 and $\delta^{60}Ni_{SRM986}$ = +0.36 ± 0.07 ‰ for NOD P1 (Gueguen et al., 2013). Internal errors of the instrumental analyses, propagated through the double spike algebra, are given in Table S1 to S3. The uncertainties on Zn and Ni isotope compositions shown on all figures are either the internal or the long-term error, whichever is larger. Three samples have been processed and analyzed as procedural duplicates. The differences between the duplicates were 0 – 0.02‰ for δ^{66}Zn and 0.02 – 0.12‰ for δ^{60}Ni, consistent with the reproducibility of pure isotope standards (Table S1 and S3). As part of the GEOTRACES intercalibration exercise, our laboratory has

demonstrated agreement for Zn and Ni isotope compositions with GEOTRACES stations (SAFE D1 and D2) (Zhao et al., 2014; Sieber et al., 2020) and USGS standard reference materials (NOD A1 and P1) (Little et al., 2020, Sun et al., 2021).

For Pb isotope analysis, samples and the Pb standard NIST SRM 981 were doped with Tl standard NIST SRM 997 to yield a Pb/Tl ratio of ~4:1. All solutions were run at ~ 20ppb Pb in 0.3 M HNO_3. Instrumental mass bias was corrected using Tl as described in Süfke et al. (2019). On a session-by-session basis, the $^{205}Tl/^{203}Tl$ ratios of the NIST 997 Tl standard was adjusted so that the average mass bias corrected Pb isotope ratios of NIST SRM 981 matched the published compositions of Baker et al. (2004). The external uncertainties were estimated based on replicate mass spectrometric sample analyses and whole procedural duplicates, and are 77 ppm for $^{206}Pb/^{204}Pb$, 108 ppm for $^{207}Pb/^{204}Pb$, 133 ppm for $^{208}Pb/^{204}Pb$, 37 ppm for $^{208}Pb/^{207}Pb$ and 27 ppm for $^{206}Pb/^{207}Pb$ (Tables S1 and S2).

3. Results

3.1. The eastern North Atlantic coastal region

3.1.1. Bulk aerosols

Bulk aerosol data are from the Senegalese (AWA) and Moroccan (EPURE) coasts (Fig. 1). We first use EFs to characterize the degree of enrichment of a TM relative to the UCC. Four samples from EPURE-Dak (orange diamonds) have EFs ~ 1 for Pb (Fig. 2a), Zn (Fig. 3a) and Ni (Fig. 4a), suggesting that these samples are strongly influenced by a natural atmospheric source, such as Saharan mineral dusts. Other bulk samples from the AWA and EPURE projects are characterized by much higher EFs, reaching ~ 300, 110 and 20 for Pb, Zn and Ni respectively. This large range of EFs indicates variable anthropogenic TM contributions, which often dominate over natural sources.

The $^{206}Pb/^{207}Pb$ and $^{208}Pb/^{207}Pb$ ratios of bulk aerosol samples from AWA range from 1.1480 to 1.1706 and from 2.4276 to 2.4403, overlapping with the range of EPURE samples (1.1519 - 1.1860, 2.4304 - 2.4814). The four EPURE-Dak samples with EF_{Pb} ~ 1, display higher $^{206}Pb/^{207}Pb$ (from 1.1706 to 1.1860) and $^{208}Pb/^{207}Pb$

ratios (from 2.4562 to 2.4814) than other bulk samples with $EF_{Pb} > 5$ (Fig. 2a). Most of the samples are correlated in $^{206}Pb/^{207}Pb$ versus $^{208}Pb/^{207}Pb$ space (r = 0.95, p-value < 0.01), but several AWA samples (U7, E10, A5 and A9) lie significantly above this correlation, towards relative enrichment in ^{206}Pb (Fig. 2 and S1).

No significant differences in $\delta^{66}Zn_{JMC\text{-}Lyon}$ were determined between AWA and EPURE, with ranges from -0.09‰ to 0.17‰ and -0.12‰ to 0.22‰, respectively (Fig. 3a). The mineral dust dominated EPURE-Dak samples, with $EF_{Zn} \sim 1$, show $\delta^{66}Zn_{JMC\text{-}Lyon}$ values that are among the highest of all aerosol samples (0.18‰ to 0.22‰, Fig. 3a).

The $\delta^{60}Ni_{SRM986}$ values range from -0.18‰ to 0.42‰ for AWA-E&U (2013) and from -0.40‰ to 0.58‰ for EPURE bulk aerosol samples (Fig. 4). Most of these samples display a strong correlation between Ni and V loadings (r = 0.98, p-value < 0.01; Fig. 5d). AWA-A (2014) samples, however, deviate from this relationship towards higher Ni (Fig. 5d). This results in distinctly low V/Ni ratios at relatively low $\delta^{60}Ni_{SRM986}$ (-0.19‰ to 0.31‰, Fig. 4b). The $\delta^{60}Ni_{SRM986}$ values of the four EPURE-Dak samples, with $EF_{Ni} \sim 1$, range from -0.17‰ to 0.05‰ (Fig. 4a), and lie in the middle of the range observed for more Ni enriched samples.

3.1.2. Water leachates

Water leachates likely access the most anthropogenically-influenced aerosol fractions, given the latter's higher solubility (Mahowald et al., 2018). The leachates from AWA have among the lowest observed Pb isotope ratios ($^{206}Pb/^{207}Pb$ ratios from 1.1463 to 1.1553 and $^{208}Pb/^{207}Pb$ ratios ranging from 2.4255 to 2.4320, Fig. 2), and variable $\delta^{66}Zn_{JMC\text{-}Lyon}$, ranging from -0.21‰ to 0.13‰ (Fig. 3). The $\delta^{60}Ni_{SRM986}$ values of the AWA leachates are separated into two groups. One group shows very high values (0.64‰ to 0.83‰) while the other is similar to soil samples and characterized by distinctly low V/Ni ratios (-0.12‰ to 0‰, V/Ni < 0.5; Fig. 4).

3.2. The higher latitude North Atlantic region

3.2.1. Water leachates

GEOVIDE leachates are more homogeneous in $\delta^{66}Zn_{JMC\text{-}Lyon}$ (-0.07‰ to 0.03‰; Fig. 3) than the coastal regions of the eastern North Atlantic. These isotope compositions are generally lighter compared to mineral dust (average of 0.24‰; Dong et al., 2013; Schleicher et al., 2020).

3.2.2. Rainwaters

Rainwater samples all come from the GEOVIDE transect. The $\delta^{66}Zn_{JMC\text{-}Lyon}$ range from -0.11‰ to 0.19‰ (Fig. 3). One sample collected near the Canadian coast (geor-10) was analyzed for Pb isotopes and has a high $^{206}Pb/^{207}Pb$ ratio (1.1650). One sample collected near Portugal (geor-3) was analyzed for Ni isotopes and shows a much lower $\delta^{60}Ni_{SRM986}$ (-0.85‰) than other atmospheric samples.

4. Discussion

The coastal North African aerosol data we present here is from a geographically-restricted area. However, these data further characterize Ni and Zn isotope compositions associated with quite general natural and anthropogenic processes leading to aerosol production, adding to a scarce database on aerosol sources, and using metal enrichment factors to help deconvolve multiple processes and sources. Furthermore, in the discussion below we combine the stable metal isotope with Pb isotope data, allowing us to add a traceable source dimension to the discussion. We also combine the new data with literature data, to get as general a picture as is currently possible of circum-North Atlantic natural and anthropogenic aerosol sources. We then assess the open ocean data in the context of this picture, integrating three different isotope tracers as well as elemental ratios.

4.1. Identifying potential aerosol sources

Natural aerosol sources can be identified using aerosol samples with relative elemental abundances close to the UCC (EF ~ 1). Anthropogenic aerosol sources, on the other hand, can be characterized using bulk aerosols with high enrichment factors (EFs > 10; Shelley et al., 2016, 2017) and the chemistry of water leachates, given the

high solubility of aerosols of anthropogenic origin (Mahowald et al., 2018). We combine EFs, specific elemental ratios and Pb isotope compositions to identify anthropogenic sources of Ni and Zn. To do so, we first discuss the origin of Pb, which has been the subject of many earlier studies, in the analyzed bulk aerosols and in leachates.

4.1.1. Source identification for the eastern North Atlantic coasts

4.1.1.1. Pb isotope evidence for contributions from easterly and westerly winds

Aerosols with crustal elemental abundances (EF ~ 1, represented by four EPURE-Dak samples, orange diamonds, Fig. 2a) have relatively high $^{206}Pb/^{207}Pb$ and $^{208}Pb/^{207}Pb$ ratios. Similar but higher Pb isotope values have previously been reported for Saharan mineral dust ($^{206}Pb/^{207}Pb$ ratios: 1.1966 to 1.2212, $^{208}Pb/^{207}Pb$ ratios: 2.4804 to 2.5138; Abouchami et al., 2013; Schleicher et al., 2020). In contrast to mineral dust, the Pb-enriched bulk aerosols and leachates from AWA and EPURE have low $^{206}Pb/^{207}Pb$ and $^{208}Pb/^{207}Pb$ ratios, as low as 1.145 and 2.245, consistent with previous observations on aerosol leachates (Bollhöfer and Rosman, 2001; Witt et al., 2006; Kumar et al., 2014; Bridgestock et al., 2016; Kumar et al., 2018). Most AWA and EPURE aerosols from the eastern North Atlantic Ocean show Pb isotope compositions that are consistent with mixing between Saharan mineral dust and anthropogenic emissions supplied through easterly winds (blue shaded area in Fig. 2b). However, a tendency towards slightly higher $^{206}Pb/^{207}Pb$ ratios is observed for some aerosol samples, in particular for AWA-U7, -E10, -A5 and -A9 from the Senegalese coast (Fig. 2 and S1). The wind back trajectory analyses (by HYSPLIT, GDAS data set; Stein et al., 2015) at these locations during sampling indicate wind directions from the northwest (Fig. S1), tentatively suggesting potential aerosol contributions from North America transported by westerly winds (green shaded area in Fig. 2b; Bollhöfer and Rosman, 2001; Noble et al., 2015).

4.1.1.2. Contributions of Saharan mineral dust to Zn and Ni budgets

Mineral dust influenced aerosols from EPURE-Dak (EF ~ 1, high $^{206}Pb/^{207}Pb$ and

$^{208}Pb/^{207}Pb$ ratios, Fig. 2a) have moderate $\delta^{66}Zn_{JMC\text{-}Lyon}$ (~ 0.2‰, Fig. 3a) and $\delta^{60}Ni_{SRM986}$ (-0.2‰ to 0.1‰, Fig. 4a), consistent with mineral dust/soil isotope compositions reported in the literature ($\delta^{66}Zn_{JMC\text{-}Lyon}$ of 0‰ to 0.4‰, Schleicher et al., 2020; $\delta^{60}Ni_{SRM986}$ of -0.33‰ to 0.32‰, Estrade et al., 2015; Ratié et al., 2015, 2018; Wu et al., 2022). Saharan dust activity is highly variable, moving with the position of the seasonally migrating intertropical convergence zone (ITCZ) and determined by the strength of the trade winds, with generally higher dust loadings during summer and winter periods (e.g., Ben-Ami et al., 2012). In the EPURE time series, the mineral dust fingerprint is best seen in December in Dakhla (orange diamonds in Fig. S2), when atmospheric Al is at its maximum. The Eastern Atlantic is the area most significantly affected by Saharan dust, whose influence is mainly dispersed across lower latitude regions (e.g., < 30°N; Jickles et al., 2005). Enrichment factors close to 1 for Ni, Zn and Pb, with high atmospheric Al loadings for aerosol samples under a North African source regime, suggest that anthropogenic aerosol contributions become less significant compared to mineral dust with strong dust activity (high Al; Figs. 5a, b, c). The Saharan mineral dust impact becomes less significant in high latitude regions (e.g., GEOVIDE; Shelley et al., 2017) and areas under a North American source regime (e.g., western part of GA03, US-GEOTRACES cruise in the equatorial North Atlantic; Shelley et al., 2015), implying spatial heterogeneity in the North Atlantic (Figs. 5a, b, c).

4.1.1.3. Zn isotope evidence for industrial and traffic emissions

The Zn-enriched bulk aerosol samples and leachates, characterized by low Pb isotope ratios, display $\delta^{66}Zn_{JMC\text{-}Lyon}$ from -0.21‰ to 0.17‰ (Fig. 3). This range overlaps with non-exhaust traffic emissions (e.g., tires and brakes) that also show moderate $\delta^{66}Zn_{JMC\text{-}Lyon}$ (-0.1‰ to 0.6‰, mean value at 0.16‰; Dong et al., 2017; Souto-Oliveira et al., 2018; Schleicher et al., 2020; Jeong et al., 2022; Schleicher and Weiss, 2023). This potential source is further supported by data from a recent study of an Irish peatland, in which urban pollution (mainly traffic) resulted in a trend towards a similar Zn isotopic end-member after 1980 (Fig. 3b; Rosca et al., 2019). Other

anthropogenic sources with a moderate $\delta^{66}Zn_{JMC\text{-}Lyon}$ range include road dust and furniture, construction (Souto-Oliveira et al., 2018, 2019), raw ore materials and their purified products, health products (John et al., 2007), and/or fertilizers (Chen et al., 2008). Thus, it is also probable that these low-temperature emissions from surrounding urban areas make significant contributions to the eastern North Atlantic coasts.

Lower $\delta^{66}Zn_{JMC\text{-}Lyon}$, as low as -0.21‰, beyond the range of the above-described intermediate isotopic end-member (Fig. 3), suggests contributions from combustion sources from high-temperature evaporation ($\delta^{66}Zn_{JMC\text{-}Lyon}$ as low as -0.73‰, mean value at -0.18‰; Schleicher et al., 2020), including at least waste incineration and industrial smelting processes (e.g., Cloquet et al., 2006; Mattielli et al., 2009; Shiel et al., 2010; Gelly et al., 2019). The overall moderate to low $\delta^{66}Zn_{JMC\text{-}Lyon}$ of our samples (-0.21‰ to 0.22‰) indicate that coal and biomass burning are not major aerosol sources in the coastal eastern North Atlantic, which should result in much higher aerosol $\delta^{66}Zn_{JMC\text{-}Lyon}$ up to 0.80‰ (Schleicher and Weiss, 2023).

4.1.1.4. Ni isotope evidence for oil combustion and lithogenic particles

Nickel isotope compositions and V/Ni ratios in Ni-enriched bulk aerosols and leachates are used to distinguish anthropogenic Ni sources (Fig. 4). Except for the mineral dust, no other end-member is clearly identified in relationships between Ni and Pb or Zn isotopes, suggesting different anthropogenic sources or fractionation mechanisms between Ni and Zn or Pb. Most aerosols from the coastal eastern North Atlantic (excluding AWA-A, Fig. 5d) are characterized by a good Ni-V correlation ($r = 0.98$, p-value < 0.01; Fig. 5d) and high $\delta^{60}Ni_{SRM986}$ in bulk sample and leachates (> 0.4‰, Fig. 4a). Both these features indicate an impact of crude oil ($\delta^{60}Ni_{SRM986}$ = 0.42‰ to 0.75‰; Ventura et al., 2015; Takano et al., 2021), in agreement with previous studies showing that shipping exhausts are an important Ni source (Becagli et al., 2012; Baker and Jickells, 2017). Most bulk EPURE-Ag samples (yellow pentagons in Fig. 4) show some contributions from a crude oil end-member, which can be explained by the proximity of Agadir to oil refineries (Rodríguez et al., 2011).

The other Ni-enriched end-member is represented by bulk samples and leachates of AWA-A, showing distinctly low V/Ni (as low as 0.2) and $\delta^{60}Ni_{SRM986}$ as low as -0.18‰ (Fig. 4). These isotope signatures are consistent with rocks/soils and laterite ores ($\delta^{60}Ni_{SRM986}$ = -0.61‰ to 0.32‰; Ratié et al., 2016, 2018). Laterite is an important Ni-enriched terrestrial weathering product and can be used as raw material for industrial production of Ni (Ratié et al., 2016). The low $^{206}Pb/^{207}Pb$ ratios (1.1533 – 1.1637) of these samples may also support their anthropogenic origin (Table S1). Meanwhile, the higher aerosol optical depth (AOD) values during AWA-A (2014) imply higher dust loadings than during AWA-E&U in 2015 (Fig. 1c, d). Aeolian erosion of Ni-enriched soils (e.g., laterite) and/or emission due to industrial processing of (lateritic) ores may account for this end-member, but this inference needs to be further investigated with more data.

Lastly, it is also possible that there are other, as yet unidentified, Ni end-members controlling aerosol samples. For example, sample Ag40 from Agadir displays relatively low $\delta^{60}Ni_{SRM986}$ at -0.40‰, with different V-Ni relationships compared to AWA-A samples (Fig. 4b). The origin of this sample remains unclear. Overall, the observation indicates highly heterogeneous Ni isotopic end-members in the atmosphere.

4.1.2. Source identification for the higher latitude North Atlantic region

Here only one rainwater sample, GEOVIDE-geor-10, located near the Canadian coast was analyzed for Pb isotopes, whose wind back trajectory analysis suggests contributions from North America (Shelley et al., 2016). The high $^{206}Pb/^{207}Pb$ compared to the correlation observed at the eastern North Atlantic coast is consistent with a main contribution from westerlies (Fig. 2b).

The $\delta^{66}Zn_{JMC\text{-}Lyon}$ variations for GEOVIDE leachates and rainwaters are from -0.11‰ to 0.19‰ (Fig. 3). The similarly moderate to low $\delta^{66}Zn_{JMC\text{-}Lyon}$ as for the AWA and EPURE samples suggest contributions mainly from metal industrial and traffic emissions, without significant impact from coal or biomass burning (e.g., Schleicher and Weiss, 2023).

A much lower $\delta^{60}Ni_{SRM986}$ than anywhere else has been observed in rain from Portugal (rainwater sample GEOVIDE-geor-3, -0.85‰), suggesting highly heterogeneous local Ni sources. This low $\delta^{60}Ni_{SRM986}$ probably cannot be produced by evaporation like Zn isotopes, given its high boiling point (2913°C; Ratié et al., 2016). The low $\delta^{60}Ni_{SRM986}$ may be linked to magmatic sulfides (-1.04‰ to -0.10‰; Gueguen et al., 2013; Hofmann et al., 2014), resulting from industrial processing of sulfide ores, or unconstrained high latitude dust sources (Fig. 4). Mixing towards an end-member with $\delta^{60}Ni_{SRM986}$ as low as -0.6‰ has also been observed in snows from Japan, but its origin remains unclear (Fig. 4; Takano et al., 2021).

4.2. Spatial aerosol source variations in the North Atlantic Ocean

Moderate to low $\delta^{66}Zn_{JMC\text{-}Lyon}$ values (< 0.6‰) were observed among our samples (-0.21‰ to 0.22‰) and for other aerosols/leachates in the open Eastern Atlantic (-0.14‰ to 0.54‰; Dong et al., 2015; Little et al., 2014; Packman et al., 2022), as well as $PM_{2.5}$ and PM_{10} aerosols in London (-0.29‰ to 0.33‰; Dong et al., 2017), Barcelona (-0.83‰ to -0.45‰; Ochoa Gonzalez et al.; 2016) and São Paulo (-1.36‰ to 0.18‰; Souto-Oliveira et al., 2019), suggesting little isotopic contrast between different Zn pollution source regimes (Fig. 3a). Therefore, traffic and metal industrial emission would be expected as the main anthropogenic Zn source to aerosols throughout the North Atlantic, characterized by light Zn isotope signals.

On the other hand, Ni shows significant local heterogeneity. The good correlation between Ni and V for aerosols and their leachates from GEOVIDE, AWA (excluding AWA-A) and EPURE is consistent with mixing towards an oil combustion end-member in the North Atlantic ($r = 0.98$, p-value < 0.01; 5d). However, GA03 samples, collected under a North American source regime, yield higher Ni/V ratios at low V loadings, producing a second trend in Ni vs V (Fig. 5d). This observation might suggest variable crude oil compositions, yet their $\delta^{60}Ni_{SRM986}$ should be similarly high (> 0.4‰) for the oil burning end-member (Ventura et al., 2015; Takano et al., 2021). Moreover, local rain samples from Portugal can be quite different in $\delta^{60}Ni_{SRM986}$, whose origin and potential impact remains to be further investigated.

4.3. The impacts of atmospheric deposition on surface seawater

4.3.1. Impacts on Pb in the surface North Atlantic Ocean

Deposition of anthropogenic aerosols is an important source of Pb to the surface ocean (e.g., Boyle et al., 2014), and we here assess the impact on Zn and Ni and their isotopes with reference to the better-studied Pb system. As noted in section 4.1.1, the Pb isotope ratios of AWA and EPURE aerosols from the eastern North Atlantic Ocean mainly reflect mixing between Saharan mineral dust and anthropogenic emissions from Europe and Africa (Fig. 2b). The natural Saharan mineral dust endmember can be estimated using average literature data ($^{206}Pb/^{207}Pb$ = 1.2102; $^{208}Pb/^{207}Pb$ = 2.5055; n = 12; Abouchami et al., 2013; Schleicher et al., 2010). The AWA leachates permit an estimation of the Pb isotope composition of the anthropogenic aerosol endmember supplied by easterly winds from Europe and Africa (mean ratios of the AWA leachates for $^{206}Pb/^{207}Pb$ = 1.1509; $^{208}Pb/^{207}Pb$ = 2.4288; n = 6), although some previous observations may indicate that even lower ratios could be chosen (e.g., Bollhöfer and Rosman, 2001). Some of the recent surface seawater samples from the Eastern Atlantic are also consistent with mixing between these two end-members, with mineral dust Pb contributions from ~ 10% to ~ 50% (Noble et al., 2015; Bridgestock et al., 2016, 2018; Zurbrick et al., 2018). Contributions from the westerlies result in higher $^{206}Pb/^{207}Pb$ in aerosols and seawater, deviating from the mixing line and exceeding the range of values measured in our study (Noble et al., 2015; Bridgestock et al., 2016, 2018; Zurbrick et al., 2018). Contributions to Pb that are 10-50% from mineral dust is broadly consistent with other estimates suggesting that 30–50% of Pb in surface waters comes from natural sources (Bridgestock et al., 2016).

4.3.2. Atmospheric deposition as an important source of isotopically light Zn to the surface ocean

Bulk aerosol data highlight a strong relationship between the natural logarithms of EFs of Zn and Pb ($r = 0.87$, p-value < 0.01; Fig. 6a), suggesting coupled transport in the atmosphere. However, Zn solubility tends to be greater than that of Pb (Shelley

et al., 2018). Indeed, aerosol leachates and rainwaters with lower Al/Pb ratios generally display similar to much higher Zn/Pb ratios compared to Saharan dust and UCC, implying that soluble Zn is equally or preferentially released compared to Pb from anthropogenic aerosols (Fig. 6c). Furthermore, soluble Zn/Pb molar ratios in both leachates and rainwaters are ≥ 10, often much higher than that of surface seawater (Fig. 6c), suggesting that the impact of atmospheric soluble depositions derived from anthropogenic aerosol must be even more significant for surface ocean Zn than it is for Pb.

As both aerosol/rainwater and seawater data are available for GEOVIDE, we estimate the turnover times of Zn in the surface ocean relative to atmospheric soluble depositions along the GEOVIDE transect (see Eq. 2 for details of calculation). Turnover times are 79 – 194 days for the western section and 2 – 51 days for the eastern section (boundary at 30°W, as suggested in Shelley et al., 2017). The short turnover time associated with atmospheric Zn supply confirms that aerosol deposition is an important source of Zn in the surface. A direct comparison of $\delta^{66}Zn_{JMC\text{-}Lyon}$ among GEOVIDE water leachates, rainwaters and mixed-layer seawater samples shows that similar compositions to atmospheric depositions are observed in the mixed layer of the western section while slightly lower $\delta^{66}Zn_{JMC\text{-}Lyon}$ are observed for the eastern side (Fig. 7). This difference may be related to higher vertical particulate export fluxes for the eastern side (Fig. 7; Lemaitre et al., 2020b), possibly resulting in removal of heavy Zn isotopes (John and Conway, 2014). Alternatively, aerosol particles with lower $\delta^{66}Zn_{JMC\text{-}Lyon}$ might occur in size fractions < 20 μm, which was not collected by W41 filters in our study (Shelley et al., 2017).

The Zn-enriched global deep ocean has a rather homogeneous $\delta^{66}Zn_{JMC\text{-}Lyon}$ of 0.46 ± 0.13‰ (2SD, n = 312; Lemaitre et al., 2020a). In contrast, the highly depleted upper 100 m is strongly skewed towards light isotope compositions (Fig. 8a, data sources in caption), with 205 values out of 328 having $\delta^{66}Zn_{JMC\text{-}Lyon}$ lower than the deep ocean range (< 0.33‰), and with only 18 values out of 328 having $\delta^{66}Zn$ higher than the deep ocean range ($\delta^{66}Zn_{JMC\text{-}Lyon}$ > 0.59‰). The data in Fig. 8 highlight the likely importance of anthropogenic Zn in controlling upper ocean Zn abundances, as

proposed by Lemaitre et al. (2020a) and Liao et al. (2020). Whether such a source can explain the full range of upper ocean light isotope compositions depends on whether the end-member is taken to be the $\delta^{66}Zn_{JMC\text{-}Lyon}$ found in aerosols from oceanic regions (-0.21% to 0.54%; data sources in caption of Fig. 8a) or the values from those collected in urban areas (-1.36% to 1.01‰; data sources in caption of Fig. 8a). Further observational and modelling work will be required to properly quantify the potential role of aerosols for oceanic Zn and its isotopes.

4.3.3. Relatively limited impact on Ni cycling in the surface ocean

The enrichment factors of Ni in bulk aerosols are generally lower than those of Pb (and Zn), suggesting less significant contributions from anthropogenic Ni (Fig. 6b). The positive correlation between the logarithm of soluble Ni/Pb and Al/Pb molar ratios ($r = 0.62$, p-value < 0.01) also suggests that both natural and anthropogenic aerosols contribute to soluble Ni fractions (Fig. 6d). Specifically, the soluble Ni/Pb derived from oil combustion, a major anthropogenic Ni source in the atmosphere (e.g., Pacyna and Pacyna, 2001), is close to two orders of magnitude lower than that of Saharan dust and surface seawater (Fig. 6d), suggesting that the impact of atmospheric soluble deposition from anthropogenic aerosol is much less significant for surface ocean Ni than it is for Pb (and Zn). Consistent with this, the range of surface ocean seawater (1.40‰ to 1.74‰) is higher and distinct from aerosol $\delta^{60}Ni_{SRM986}$ (-0.85‰ to 0.83‰; data sources in caption of Fig. 8b).

5. Conclusion

In this study, we have presented new Zn, Ni and Pb isotope data from bulk aerosols, their leachates, and rainwaters collected off the Moroccan and Senegalese coasts (EPURE and AWA projects respectively), and in the higher latitude open North Atlantic Ocean (GEOVIDE project). Combining radiogenic Pb isotopes, stable metal isotope analyses, elemental ratios and elemental enrichment factors (EFs, relative to element/Al ratios of the continental crust) allow the identification of natural and anthropogenic aerosol sources, and add to the limited number of studies seeking to

fingerprint potential processes and sources for open ocean aerosols.

High dust activity off the African coast results in high atmospheric Al loadings, EF ~ 1 and low dust solubility, with isotope compositions similar to Saharan dust (high $^{206}Pb/^{207}Pb$ and $^{208}Pb/^{207}Pb$, moderate $^{66}Zn_{Lyon}$ of ~ 0.2‰ and $^{60}Ni_{SRM986}$ of -0.2‰ to 0.1‰). Conversely, anthropogenic aerosols are characterized by EFs > 10, greater solubility, low Pb isotope ratios and specific Zn and Ni isotope compositions depending on the anthropogenic source (see below).

Generally, low $^{206}Pb/^{207}Pb$ and $^{208}Pb/^{207}Pb$ ratios are observed in the eastern North Atlantic, suggesting mixing of Saharan dust with anthropogenic aerosols from Europe/North Africa supplied by easterly winds. Higher $^{206}Pb/^{207}Pb$ than the correlation defined by most of the data suggests anthropogenic aerosol contributions from North America, which is observed near the Canadian coast and occasionally in the Eastern Atlantic. Aerosol Zn isotope compositions point to anthropogenic contributions possibly from traffic and metal industrial emissions, whereby the high-temperature evaporation causes distinctly lower aerosol $\delta^{66}Zn_{JMC\text{-}Lyon}$ (as low as -0.21‰) than the average crustal value. The influence of oil combustion on aerosol Ni is widespread and recognized in relatively high $\delta^{60}Ni_{SRM986}$ values (> 0.4‰) and good correlations between Ni and V concentrations. Highly heterogenous $\delta^{60}Ni_{SRM986}$ is observed for other non-oil anthropogenic sources, whose origins are not yet fully defined.

The fact that soluble Zn/Pb ratios in anthropogenic aerosols range between 1 and 100 times those of the surface ocean, suggests an anthropogenic impact on surface ocean Zn that is as big or bigger than for Pb. Thus, the release of isotopically light Zn from anthropogenically sourced aerosol may be a key factor in determining the light Zn isotope compositions in surface seawater. However, lower $\delta^{66}Zn_{JMC\text{-}Lyon}$ is observed in the oceanic mixed layer than has yet been found in aerosols and rainwaters sampled over the ocean. This could imply that other factors control Zn isotopes in the surface ocean, or that the currently very limited sampling of oceanic aerosol is not representative. The direct impact of atmospheric input on Ni cycling in the surface ocean is insignificant, revealed by the very different $\delta^{60}Ni_{SRM986}$ measured

in aerosols/rainwater versus seawater.

Though our study has added to the data for Zn and Ni isotopes in marine aerosols, these datasets are still very small. The problem of data scarcity is particularly important given the significant heterogeneity in source signatures. We suggest that the coupling of a source tracer, such as Pb isotopes, to metal isotopes that respond more to process, is going to be crucial in understanding this source heterogeneity. In addition, such an approach allows using metal/Pb ratios to place quantitative constraints on the magnitude of the depositional flux of metals to the surface ocean. Quantitative observations along these lines will, however, also need to be coupled to atmospheric transport models, as well as models of surface ocean elemental cycling between particulates and the aqueous phase, in order to reach a more complete understanding of the importance of natural and anthropogenic aerosols on upper ocean systematics of metals, such as Zn, and their isotopes.

Acknowledgements:

We would like to thank the captains, crews and chief scientists of the GEOVIDE (Géraldine Sarthou and Pascale Lherminier), AWA (Patrice Brehmer) and EPURE (Luis Tito de Morais) projects. The GEOVIDE work was supported by the French National Research Agency (ANR-13-BS06-0014 and ANR-12-PDOC-0025-01), the French National Centre for Scientific Research (CNRS-LEFE-CYBER), Ifremer and the "Laboratoire d'Excellence" Labex-Mer (ANR-10-LABX-19). The AWA project 'Ecosystem Approach to the management of fisheries and the marine environment in West African waters' (scientific cruise doi: 10.17600/14001400) was funded by the grants 01DG12073E and 01DG1207B from the German Federal Ministry of Education and Research (BMBF) and the Institut de Recherche pour le Développement (IRD). The Franco-Moroccan EPURE project 'Eléments trace métalliques, Pollution, Upwelling et Ressources' was financially supported by the grant ANR-11-CEPL-0005, under the call CEP&S of the French National Research Agency (ANR). In addition, a grant from the Conseil Générale du Finistère (CG29) supported Rachel Shelley during the EPURE project. We are grateful to the late

Georges Tymen for collecting the aerosol samples during this latter project. Finally, Corey Archer is greatly thanked for his help and support in the lab. This research was funded by the Swiss National Science Foundation (grants 200020_165904). Nolwenn Lemaitre has received funding from the European Union under the Marie Skłodowska-Curie grant agreement 101066172 (project IsoMargin). Views and opinions expressed are however those of the authors only and do not necessarily reflect those of the European Union or the REA.A – Marie Sklodowska-Curie Actions & Support to Experts. Neither the European Union nor the granting authority can be held responsible for them. Xingchao Zhang was supported by the China Scholarship Council (grant 201906340082).

References:

Abouchami W., Näthe K., Kumar A., Galer S. J. G., Jochum K. P., Williams E., Horbe A. M. C., Rosa J. W. C., Balsam W. and Adams D. (2013) Geochemical and isotopic characterization of the Bodélé Depression dust source and implications for transatlantic dust transport to the Amazon Basin. *Earth Planet. Sci. Lett.* **380**, 112–123.

Archer C. and Vance D. (2004) Mass discrimination correction in multiple-collector plasma source mass spectrometry: an example using Cu and Zn isotopes. *J. Anal. At. Spectrom.* **19**, 656–665.

Archer C., Andersen M. B., Cloquet C., Conway T. M., Dong S., Ellwood M., Moore R., Nelson J., Rehkämper M. and Rouxel O. (2017) Inter-calibration of a proposed new primary reference standard AA-ETH Zn for zinc isotopic analysis. *J. Anal. At. Spectrom.* **32**, 415–419.

Archer C., Vance D., Milne A. and Lohan M. C. (2020) The oceanic biogeochemistry of nickel and its isotopes: New data from the South Atlantic and the Southern Ocean biogeochemical divide. *Earth Planet. Sci. Lett.* **535**, 116118.

Baker A. R. and Jickells T. D. (2017) Progress in Oceanography Atmospheric deposition of soluble trace elements along the Atlantic Meridional Transect (AMT). *Prog. Oceanogr.* **158**, 41–51.

Baker J., Peate D., Waight T. and Meyzen C. (2004) Pb isotopic analysis of standards a nd samples using a 207Pb-204Pb double spike and thallium to correct for mass bias with a double-focusing MC-ICP-MS. *Chem. Geol.* 211, 275–303.

Becagli S., Sferlazzo D. M., Pace G., Sarra A., Bommarito C., Calzolai G., Ghedini C., Lucarelli F., Lastruccia V. and Fiorentino S. (2012) Evidence for heavy fuel oil combustion aerosols from chemical analyses at the island of Lampedusa: a possible large role of ships emissions in the Mediterranean. *Atmos. Chem. Phys.* 12(7), 3479-3492.

Ben-Ami Y., Koren I., Altaratz O., Kostinski A. and Lehahn Y. (2012) Discernible rhythm in the spatio/temporal distributions of transatlantic dust. *Atmos. Chem. Phys.* **12**, 2253–2262.

Bermin J., Vance D., Archer C. and Statham P. J. (2006) The determination of the isotopic composition of Cu and Zn in seawater. *Chem. Geol.* **226**, 280–297.

Bollhöfer A. and Rosman K. J. R. (2001) Isotopic source signatures for atmospheric lead: the Northern Hemisphere. *Geochim. Cosmochim. Acta* **65**, 1727–1740.

Boyle E. A., Lee J. M., Echegoyen Y., Noble A., Moos S., Carrasco G., Zhao N., Kayser R., Zhang J., Gamo T., Obata H. and Norisuye K. (2014) Anthropogenic lead emissions in the ocean: The evolving global experiment. *Oceanography* **27**, 69–75.

Bridgestock L., Rehkämper M., van de Flierdt T., Paul M., Milne A., Lohan M. C. and Achterberg E. P. (2018) The distribution of lead concentrations and isotope compositions in the eastern Tropical Atlantic Ocean. *Geochim. Cosmochim. Acta* **225**, 36–51.

Bridgestock L., Van De Flierdt T., Rehkämper M., Paul M., Middag R., Milne A., Lohan M. C., Baker A. R., Chance R., Khondoker R., Strekopytov S.,

Humphreys-Williams E., Achterberg E. P., Rijkenberg M. J. A., Gerringa L. J. A. and De Baar H. J. W. (2016) Return of naturally sourced Pb to Atlantic surface waters. *Nat. Commun.* **7**.

Cameron V. and Vance D. (2014) Heavy nickel isotope compositions in rivers and the oceans. *Geochim. Cosmochim. Acta* **128**, 195–211. Available at: http://dx.doi.org/10.1016/j.gca.2013.12.007.

Cameron V., Vance D., Archer C. and House C. H. (2009) A biomarker based on the stable isotopes of nickel. *Proc. Natl. Acad. Sci. U. S. A.* **106**, 10944–10948.

Chen J., Gaillardet J. and Louvat P. (2008) Zinc isotopes in the Seine River waters, France: A probe of anthropogenic contamination. *Environ. Sci. Technol.* **42**, 6494–6501.

Cloquet C., Carignan J. and Libourel G. (2006) Isotopic composition of Zn and Pb atmospheric depositions in an urban/periurban area of northeastern France. *Environ. Sci. Technol.* **40**, 6594–6600.

Conway T. M. and John S. G. (2014) The biogeochemical cycling of zinc and zinc isotopes in the North Atlantic Ocean. *Glob. Biogeochem. Cycles Res.*, 1111–1128.

Conway, T. M., and John, S. G. (2015). The cycling of iron, zinc and cadmium in the North East Pacific Ocean–Insights from stable isotopes. *Geochimica et Cosmochimica Acta* 164, 262-283.

Dong S., Gonzalez R. O., Harrison R. M., Green D., North R., Fowler G. and Weiss D. (2017) sources for copper and zinc in aerosols in London , United Kingdom. *Atmos. Environ.*

Dong S., Weiss D. J., Strekopytov S., Kreissig K., Sun Y., Baker A. R. and Formenti P. (2013) Stable isotope ratio measurements of Cu and Zn in mineral dust (bulk and size fractions) from the Taklimakan Desert and the Sahel and in aerosols from the eastern tropical North Atlantic Ocean. *Talanta* **114**, 103–109.

Estrade N., Cloquet C., Echevarria G., Sterckeman T., Deng T., Tang Y. T. and Morel J. L. (2015) Weathering and vegetation controls on nickel isotope fractionation in surface ultramafic environments (Albania). *Earth Planet. Sci. Lett.* 423, 24–35.

Gall L., Williams H. M., Halliday A. N. and Kerr A. C. (2017) Nickel isotopic composition of the mantle. *Geochim. Cosmochim. Acta* **199**, 196–209.

Gelly R., Fekiacova Z., Guihou A., Doelsch E., Deschamps P. and Keller C. (2019) Lead, zinc, and copper redistributions in soils along a deposition gradient from emissions of a Pb-Ag smelter decommissioned 100 years ago. *Sci. Total Environ.* **665**, 502–512.

Gonzalez R. O., Strekopytov S., Amato F., Querol X., Reche C. and Weiss D. (2016) New Insights from Zinc and Copper Isotopic Compositions into the Sources of Atmospheric Particulate Matter from Two Major European Cities. *Environ. Sci. Technol.* **50**, 9816–9824.

Gueguen B., Rouxel O., Ponzevera E., Bekker A. and Fouquet Y. (2013) Nickel isotope variations in terrestrial silicate rocks and geological reference materials measured by MC-ICP-MS. *Geostand. Geoanalytical Res.* **37**, 297–317.

Hamilton D. S., Perron M. M. G., Bond T. C., Bowie A. R., Buchholz R. R., Guieu C., Ito A., Maenhaut W., Myriokefalitakis S., Olgun N., Rathod S. D., Schepanski K., Tagliabue A., Wagner R. and Mahowald N. M. (2022) Earth, Wind, Fire, and Pollution: Aerosol Nutrient Sources and Impacts on Ocean Biogeochemistry. *Ann. Rev. Mar. Sci.* 14, 303–330.

Hatta, M., Measures, C.I., Roshan, S., Wu, J., Fitzsimmons, J.N., Sedwick, P., Morton, P., (2015) An overview of dissolved Fe and Mn distributions during the 2010-2011 U.S. GEOTRACES North Atlantic Cruises: GEOTRACES GA03. Deep Sea Res. Part II: Topical Stud. Oceanogr. 116, 117–129.

Hofmann A., Bekker A., Dirks P., Gueguen B., Rumble D. and Rouxel O. J. (2014) Comparing orthomagmatic and hydrothermal mineralization models for komatiite-hosted nickel deposits in Zimbabwe using multiple-sulfur, iron, and nickel isotope data. *Miner. Depos.* **49**, 75–100.

Ito A., Myriokefalitakis S., Kanakidou M., Mahowald N. M., Scanza R. A., Hamilton D. S., Baker A. R., Jickells T., Sarin M., Bikkina S., Gao Y., Shelley R. U., Buck C. S., Landing W. M., Bowie A. R., Perron M. M. G., Guieu C., Meskhidze N., Johnson M. S., Feng Y., Kok J. F., Nenes A. and Duce R. A. (2019) Pyrogenic iron: The missing link to high iron solubility in aerosols. *Sci. Adv.* 5, 13–15.

Jeong H. and Ra K. (2021) Multi-isotope signatures (Cu, Zn, Pb) of different particle sizes in road-deposited sediments: a case study from industrial area. *J. Anal. Sci. Technol.* **12**.

Jeong, H., Ryu, J.S., Ra, K., 2022. Characteristics of potentially toxic elements and multiisotope signatures (Cu, Zn, Pb) in non-exhaust traffic emission sources. *Environ. Pollut.* 292.

Jickells T. D., An Z. S., Andersen K. K., Baker A. R., Bergametti C., Brooks N., Cao J. J., Boyd P. W., Duce R. A., Hunter K. A., Kawahata H., Kubilay N., LaRoche J., Liss P. S., Mahowald N., Prospero J. M., Ridgwell A. J., Tegen I. and Torres R. (2005) Global iron connections between desert dust, ocean biogeochemistry, and climate. *Science* **308**, 67–71.

John S. G. and Conway T. M. (2014) A role for scavenging in the marine biogeochemical cycling of zinc and zinc isotopes. *Earth Planet. Sci. Lett.* 394, 159–167.

John S. G., Helgoe J. and Townsend E. (2018) Biogeochemical cycling of Zn and Cd and their stable isotopes in the Eastern Tropical South Paci fi c. *Mar. Chem.* **201**, 256–262.

John S. G., Park J. G., Zhang Z. and Boyle E. A. (2007) The isotopic composition of some common forms of anthropogenic zinc. *Chem. Geol.* **245**, 61–69.

Komárek M., Ettler V., Chrastný V. and Mihaljevič M. (2008) Lead isotopes in environmental sciences: A review. *Environ. Int.* **34**, 562–577.

König D., Conway T. M., Hamilton D. S. and Tagliabue A. (2022) Surface Ocean Biogeochemistry Regulates the Impact of Anthropogenic Aerosol Fe Deposition on the Cycling of Iron and Iron Isotopes in the North Pacific. *Geophys. Res. Lett*. 49(13), e2022GL098016.

Kumar A., Abouchami W., Galer S. J. G., Garrison V. H., Williams E. and Andreae

M. O. (2014) A radiogenic isotope tracer study of transatlantic dust transport from Africa to the Caribbean. *Atmos. Environ.* **82**, 130–143.

Kumar A., Abouchami W., Galer S. J. G., Singh S. P., Fomba K. W., Prospero J. M. and Andreae M. O. (2018) Seasonal radiogenic isotopic variability of the African dust outflow to the tropical Atlantic Ocean and across to the Caribbean. *Earth Planet. Sci. Lett.* **487**, 94–105.

Lemaitre N., de Souza G. F., Archer C., Wang R. M., Planquette H., Sarthou G. and Vance D. (2020a) Pervasive sources of isotopically light zinc in the North Atlantic Ocean. *Earth Planet. Sci. Lett.* **539**, 116216.

Lemaitre N., Du J., de Souza G. F., Archer C. and Vance D. (2022) The essential bioactive role of nickel in the oceans: Evidence from nickel isotopes. *Earth Planet. Sci. Lett.* **584**, 117513. Available at: https://doi.org/10.1016/j.epsl.2022.117513.

Lemaitre N., Planquette H., Dehairs F., Planchon F., Sarthou G., Gallinari M., Roig S., Jeandel C. and Castrillejo M. (2020b) Particulate Trace Element Export in the North Atlantic (GEOTRACES GA01 Transect: GEOVIDE Cruise). *ACS Earth Sp. Chem.* 4, 2185–2204.

Liao W. H., Takano S., Yang S. C., Huang K. F., Sohrin Y. and Ho T. Y. (2020) Zn Isotope Composition in the Water Column of the Northwestern Pacific Ocean: The Importance of External Sources. *Global Biogeochem. Cycles* **34**.

Liao W.-H., Takano S., Tian H.-A., Chen H.-Y., Sohrin Y. and Ho T.-Y. (2021) Zn elemental and isotopic features in sinking particles of the South China Sea: Implications for its sources and sinks. *Geochim. Cosmochim. Acta* **314**, 68–84.

Little S. H., Archer C., McManus J., Najorka J., Wegorzewski A. V. and Vance D. (2020) Towards balancing the oceanic Ni budget. *Earth Planet. Sci. Lett.* **547**, 116461.

Little S. H., Vance D., Walker-Brown C. and Landing W. M. (2014) The oceanic mass balance of copper and zinc isotopes, investigated by analysis of their inputs, and outputs to ferromanganese oxide sediments. *Geochim. Cosmochim. Acta* **125**, 673–693.

Lugmair G. W. and Galer S. J. G. (1992) Age and isotopic relationships among the angrites Lewis Cliff 86010 and Angra dos Reis. *Geochim. Cosmochim. Acta* **56**, 1673–1694.

Mahowald N. M., Hamilton D. S., Mackey K. R. M., Moore J. K., Baker A. R., Scanza R. A. and Zhang Y. (2018) Aerosol trace metal leaching and impacts on marine microorganisms. *Nat. Commun.* **9**.

Marsay C. M., Landing W. M., Umstead D., Till C. P., Freiberger R., Fitzsimmons J. N., Lanning N. T., Shiller A. M., Hatta M., Chmiel R., Saito M., Buck, C. S. (2022) Does Sea Spray Aerosol Contribute Significantly to Aerosol Trace Element Loading? A Case Study From the US GEOTRACES Pacific Meridional Transect (GP15). *Global Biogeochem. Cycles* 36(8), e2022GB007416.

Mattielli N., Petit J. C. J., Deboudt K., Flament P., Perdrix E., Taillez A., Rimetz-Planchon J. and Weis D. (2009) Zn isotope study of atmospheric emissions and dry depositions within a 5 km radius of a Pb-Zn refinery. *Atmos.*

Environ. **43**, 1265–1272.

Menzel Barraqueta, J.-L., Schlosser, C., Planquette, H., Gourain, A., Cheize, M., Boutorh, J., Shelley, R., Pereira Contreira, L., Gledhill, M., Hopwood, M. J., Lherminier, P., Sarthou, G., and Achterberg, E. P. (2018) Aluminium in the North Atlantic Ocean and the Labrador Sea (GEOTRACES GA01 section): roles of continental inputs and biogenic particle removal, Biogeosciences 15(16): 5271-5286.

Morel F. M. M. and Price N. M. (2003) The biogeochemical cycles of trace metals in the oceans. *Science.* **300**, 944–947.

Naidja L., Ali-Khodja H. and Khardi S. (2018) Sources and levels of particulate matter in North African and Sub-Saharan cities: a literature review. *Environ. Sci. Pollut. Res.* **25**, 12303–12328.

Noble A. E., Echegoyen-sanz Y., Boyle E. A., Ohnemus D. C., Lam P. J., Kayser R., Reuer M., Wu J. and Smethie W. (2015) Dynamic variability of dissolved Pb and Pb isotope composition from the U . S . North Atlantic GEOTRACES transect. *Deep-sea Res. Pt. II* **116**, 208–225.

Packman H., Little S. H., Baker A. R., Bridgestock L., Chance R. J., Coles B. J., Kreissig K., Rehkämper M. and van de Flierdt T. (2022) Tracing natural and anthropogenic sources of aerosols to the Atlantic Ocean using Zn and Cu isotopes. *Chem. Geol.* 121091.

Pacyna J. M. and Pacyna E. G. (2001) An assessment of global and regional emissions of trace metals to the atmosphere from anthropogenic sources worldwide. *Environ. Rev.* **9**, 269–298.

Petzold A., Veira A., Mund S., Esselborn M., Kiemle C., Weinzierl B., Hamburger T., Ehret G., Lieke K. and Kandler K. (2011) Mixing of mineral dust with urban pollution aerosol over Dakar (Senegal): Impact on dust physico-chemical and radiative properties. *Tellus, Ser. B Chem. Phys. Meteorol.* **63**, 619–634.

Prospero J. M., Bullard J. E. and Hodgkins R. (2012) High-latitude dust over the North Atlantic: Inputs from Icelandic proglacial dust storms. *Science.* **335**, 1078–1082.

Ratié G., Garnier J., Calmels D., Vantelon D., Guimarães E., Monvoisin G., Nouet J., Ponzevera E. and Quantin C. (2018) Nickel distribution and isotopic fractionation in a Brazilian lateritic regolith: Coupling Ni isotopes and Ni K-edge XANES. *Geochim. Cosmochim. Acta* **230**, 137–154.

Ratié G., Jouvin D., Garnier J., Rouxel O., Miska S., Guimarães E., Cruz Vieira L., Sivry Y., Zelano I., Montarges-Pelletier E., Thil F. and Quantin C. (2015) Nickel isotope fractionation during tropical weathering of ultramafic rocks. *Chem. Geol.* **402**, 68–76.

Ratié G., Quantin C., Jouvin D., Calmels D., Ettler V., Sivry Y., Vieira L. C., Ponzevera E. and Garnier J. (2016) Nickel isotope fractionation during laterite Ni ore smelting and refining: Implications for tracing the sources of Ni in smelter-affected soils. *Appl. Geochemistry* **64**, 136–145.

Rodríguez S., Alastuey A., Alonso-Pérez S., Querol X., Cuevas E., Abreu-Afonso J., Viana M., Pérez N., Pandolfi M. and De La Rosa J. (2011) Transport of desert

dust mixed with North African industrial pollutants in the subtropical Saharan Air Layer. *Atmos. Chem. Phys.* **11**, 6663–6685.

Rosca C., Schoenberg R., Tomlinson E. L. and Kamber B. S. (2019) Combined zinc-lead isotope and trace-metal assessment of recent atmospheric pollution sources recorded in Irish peatlands. *Sci. Total Environ*. 658, 234–249.

Rudnick, R.L., Gao, S. (2014) Composition of the Continental Crust. In *Treatise on Geochemistry* (eds. H. D. Holland and K. K. Turekian), 2nd ed. Elsevier, Oxford, pp. 1-51.

Schleicher N. J., Dong S., Packman H., Little S. H., Ochoa Gonzalez R., Najorka J., Sun Y. and Weiss D. J. (2020) A Global Assessment of Copper, Zinc, and Lead Isotopes in Mineral Dust Sources and Aerosols. *Front. Earth Sci.* **8**, 1–20.

Schleicher, N. J., and Weiss, D. J. (2023) Identification of atmospheric particulate matter derived from coal and biomass burning and from non-exhaust traffic emissions using zinc isotope signatures. *Environ. Pollut.* 329, 121664.

Shelley R. U., Landing W. M., Ussher S. J., Planquette H. and Sarthou G. (2018) Regional trends in the fractional solubility of Fe and other metals from North Atlantic aerosols (GEOTRACES cruises GA01 and GA03) following a two-stage leach. *Biogeosciences* **15**, 2271–2288.

Shelley R. U., Morton P. L. and Landing W. M. (2015) Elemental ratios and enrichment factors in aerosols from the US-GEOTRACES North Atlantic transects. *Deep. Res. Part II Top. Stud. Oceanogr.* **116**, 262–272.

Shelley R. U., Roca-Martí M., Castrillejo M., Sanial V., Masqué P., Landing W. M., Planquette H. and Sarthou G. (2017) Quantification of trace element atmospheric deposition fluxes to the Atlantic Ocean (>40°N; GEOVIDE, GEOTRACES GA01) during spring 2014. *Deep. Res. Part I Oceanogr. Res. Pap.* **119**, 34–49.

Shelley R., Sarthou G., Tyman C., Losno R., de Morais L. T., Benhra A. and Boutir F. Z. (2016) A case study of aerosol trace element deposition to Moroccan coastal waters. In *European Aerosol Conference (EAC 2016)* pp. 1-p.

Shiel A. E., Weis D. and Orians K. J. (2010) Evaluation of zinc, cadmium and lead isotope fractionation during smelting and refining. *Sci. Total Environ.* **408**, 2357–2368.

Sieber M., Conway T. M., de Souza G. F., Hassler C. S., Ellwood M. J. and Vance D. (2020) Cycling of zinc and its isotopes across multiple zones of the Southern Ocean: Insights from the Antarctic Circumnavigation Expedition. *Geochim. Cosmochim. Acta* **268**, 310–324.

Souto-Oliveira C. E., Babinski M., Araújo D. F. and Andrade M. F. (2018) Multi-isotopic fingerprints (Pb, Zn, Cu) applied for urban aerosol source apportionment and discrimination. *Sci. Total Environ.* **626**, 1350–1366.

Souto-Oliveira C. E., Babinski M., Araújo D. F., Weiss D. J. and Ruiz I. R. (2019) Multi-isotope approach of Pb, Cu and Zn in urban aerosols and anthropogenic sources improves tracing of the atmospheric pollutant sources in megacities. *Atmos. Environ.* **198**, 427–437.

Stein A. F., Draxler R. R., Rolph G. D., Stunder B. J. B., Cohen M. D. and Ngan F. (2015) Noaa's hysplit atmospheric transport and dispersion modeling system.

Bull. Am. Meteorol. Soc. **96**, 2059–2077.

Süfke F., Gutjahr M., Gilli A., Anselmetti F. S., Glur L. and Eisenhauer A. (2019) Early stage weathering systematics of Pb and Nd isotopes derived from a high-Alpine Holocene lake sediment record. *Chem. Geol.* **507**, 42–53.

Sun M., Archer C. and Vance D. (2021) New methods for the chemical isolation and stable isotope measurement of multiple transition metals, with application to the earth sciences. *Geostand. Geoanal. Res.* 45(4), 643-658.

Sunda W. G. (1988) Trace metal interactions with marine phytoplankton. *Biol. Oceanogr.* **6**, 411–442.

Takano S., Liao W., Tian H., Huang K. and Ho T. (2020) Sources of particulate Ni and Cu in the water column of the northern South China Sea : Evidence from elemental and isotope ratios in aerosols and sinking particles. *Mar. Chem.* **219**, 103751.

Takano S., Tsuchiya M., Imai S., Yamamoto Y., Fukami Y., Suzuki K. and Sohrin Y. (2021) Isotopic analysis of nickel, copper, and zinc in various freshwater samples for source identification. *Geochem. J.* **55**, 171–183.

Thapalia A., Borrok D. M., Van Metre P. C., Musgrove M. and Landa E. R. (2010) Zn and Cu isotopes as tracers of anthropogenic contamination in a sediment core from an urban lake. *Environ. Sci. Technol.* **44**, 1544–1550.

Vance D., Little S. H., Archer C., Cameron V., Andersen M. B., Rijkenberg M. J. A. and Lyons T. W. (2016) The oceanic budgets of nickel and zinc isotopes: The importance of sulfdic environments as illustrated by the Black Sea. *Philos. Trans. R. Soc. A Math. Phys. Eng. Sci.* **374**.

Ventura G. T., Gall L., Siebert C., Prytulak J., Szatmari P., Hürlimann M. and Halliday A. N. (2015) The stable isotope composition of vanadium, nickel, and molybdenum in crude oils. *Appl. Geochem.* **59**, 104–117.

Wang R. M., Archer C., Bowie A. R. and Vance D. (2019) Zinc and nickel isotopes in seawater from the Indian Sector of the Southern Ocean: The impact of natural iron fertilization versus Southern Ocean hydrography and biogeochemistry. *Chem. Geol.* **511**, 452–464.

Weber T., John S., Tagliabue A. and DeVries T. (2018) Biological uptake and reversible scavenging of zinc in the global ocean. *Science* 361(6397), 72-76.

Witt M., Baker A. R. and Jickells T. D. (2006) Atmospheric trace metals over the Atlantic and South Indian Oceans: Investigation of metal concentrations and lead isotope ratios in coastal and remote marine aerosols. *Atmos. Environ.* **40**, 5435–5451.

Wu G., Zhu J.-M., Wang X., Johnson T. M., He Y., Huang F., Wang L.-X. and Lai S.-C. (2022) Nickel isotopic composition of the upper continental crust. *Geochim. Cosmochim. Acta* 332, 263–284.

Yang, S.-C., Kelly, R.L., Bian, X., Conway, T.M., Huang, K.-F., Ho, T.-Y., Neibauer, J.A., Keil, R.G., Moffett, J.W., John, S.G., (2021) Lack of redox cycling for nickel in the water column of the Eastern tropical north pacific oxygen deficient zone: Insight from dissolved and particulate nickel isotopes. *Geochim. Cosmochim. Acta* 309, 235–250.

Zhang X., Huang J., Gong Y., Zhang L. and Huang F. (2022) Climate influence on zinc isotope variations in a loess–paleosol sequence of the Chinese Loess Plateau. *Geochim. Cosmochim. Acta* **321**, 115–132.

Zhao Y., Vance D., Abouchami W. and de Baar H. J. W. (2014) Biogeochemical cycling of zinc and its isotopes in the Southern Ocean. *Geochim. Cosmochim. Acta* **125**, 653–672.

Zurbrick C. M., Boyle E. A., Kayser R., Reuer M. K., Wu J., Planquette H., Shelley R., Boutorh J., Cheize M., Contreira L., Menzel Barraqueta J.-L. and Sarthou G. (2018) Dissolved Pb and Pb isotopes in the North Atlantic from the GEOVIDE transect (GEOTRACES GA-01) and their decadal evolution. Biogeosciences, 15 (16), 4995-5014.

Figure 1:

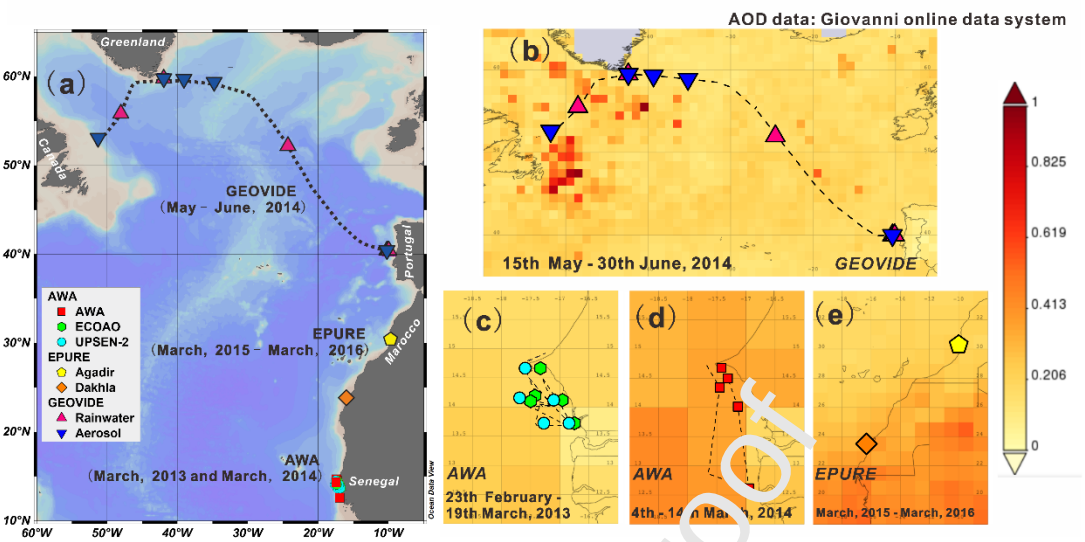

Figure 1. Sample locations in this study: (a) overview, (b) GEOVIDE project (GEOTRACES GA01 section); (c, d) AWA project including the cruises AWA (AWA-A, in red), ECOAO (AWA-E, in green) and UPSEN-2 (AWA-U, in cyan); (e) EPURE project. The overview map in (a) was produced using Ocean Data View. The background colors in panels (b) to (e) show aerosol optical depth (550 nm) averaged over the time period of the expedition, and were produced using the Giovanni online data system (http:// aeronet.gsfc.nasa.gov), NASA GES DISC70 with mean daily data from the MODIS instrument on board the Terra satellite.

Figure 2:

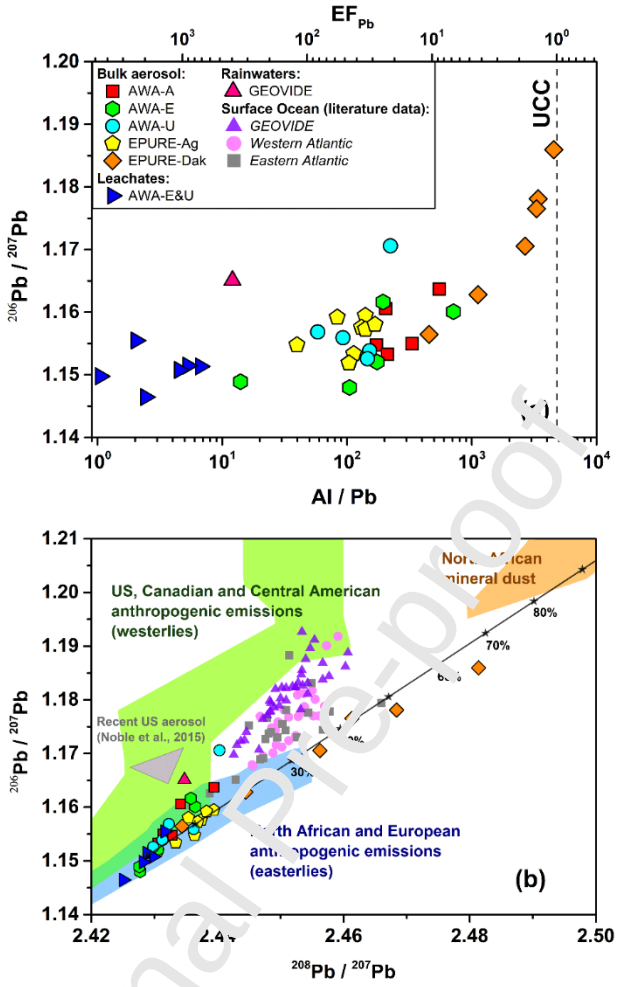

Figure 2. (a) $^{206}Pb/^{207}Pb$ versus Al/Pb ratios (bottom x-axis) and Pb enrichment factors (top x-axis, with the upper continental crust, UCC, shown by the dashed black line) and (b) Pb triple isotope plot of aerosol, UHP water leachate, rainwater and seawater data for the North Atlantic. Anthropogenic aerosols derived from North and Central America are delineated by the green shaded area, with recent US aerosols in grey (Bollhöfer et al., 2001; Noble et al., 2015); anthropogenic aerosols from North Africa and Europe are shown by the blue shaded area (Bollhöfer et al., 2001; Bridgestock et al., 2016); Saharan mineral dust is shown by the orange shaded area (Abouchami et al., 2013; Schleicher et al., 2020). Recent surface seawater data for the North Atlantic (after 2010) are from the GEOTRACES GA01 (GEOVIDE), GA02, GA03 and GA06 cruises (Noble et al., 2015; Bridgestock et al., 2016, 2018; Zubrick et al., 2018). A calculated mixing trajectory between the AWA UHP water leachates and average Saharan mineral dust (see section 4.1. for more information) is shown as the black line. Error bars are smaller than the size of the symbols.

Figure 3:

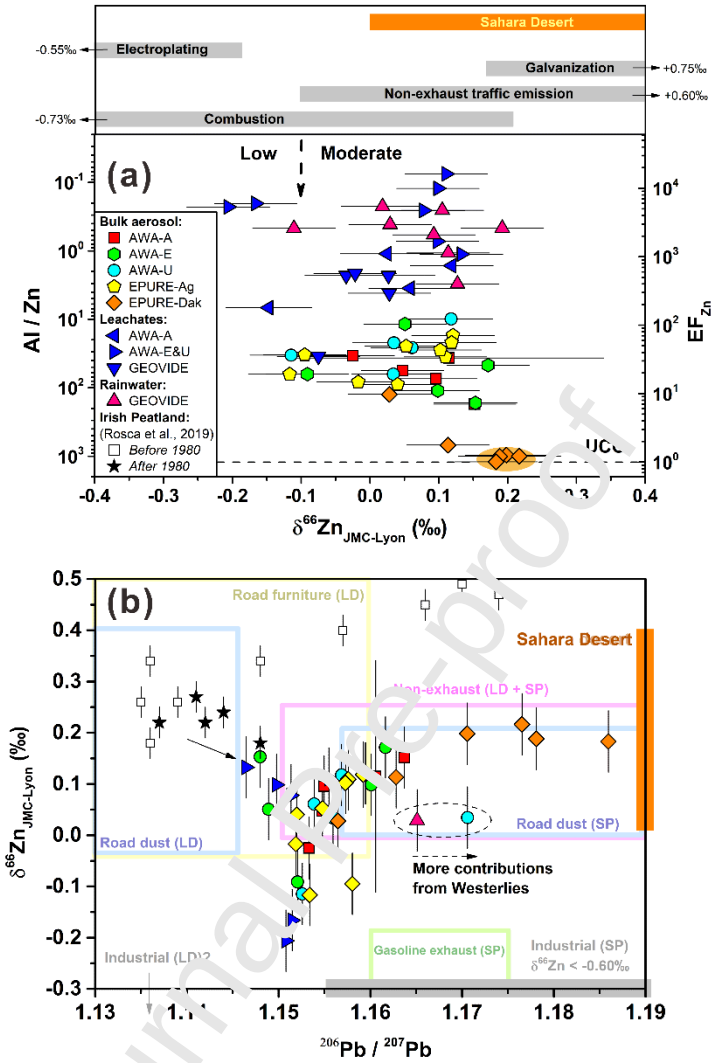

Figure 3. $\delta^{66}Zn_{JMC\text{-}Lyon}$ versus (a) Al/Zn ratios (with the upper continental crust, UCC, shown by the dashed black line) and (b) $^{206}Pb/^{207}Pb$ for aerosol, UHP water leachate and rainwater samples. Isotope compositions of aerosol endmembers are shown in the top part of (a) (Schleicher et al., 2020). Literature data for both Zn and Pb isotope compositions for an Irish peatland (bog) (Rosca et al., 2019) and anthropogenic end-members from London (LD) (Ochoa Gonzalez et al., 2016; Dong et al., 2017) and São Paulo (SP) (Souto-Oliveira et al., 2018, 2019) are shown in (b). The black arrow represents a city pollution trend (mainly traffic) in the post-1980 bog record. The dashed arrow in (a) represents the lower boundary of the intermediate Zn isotopic end-member defined in previous work (-0.10‰ to 0.60‰; Schleicher et al., 2020; Schleicher and Weiss, 2023). The dashed arrow in (b) represents potential contribution from the westerlies, with relatively higher ^{206}Pb.

Figure 4:

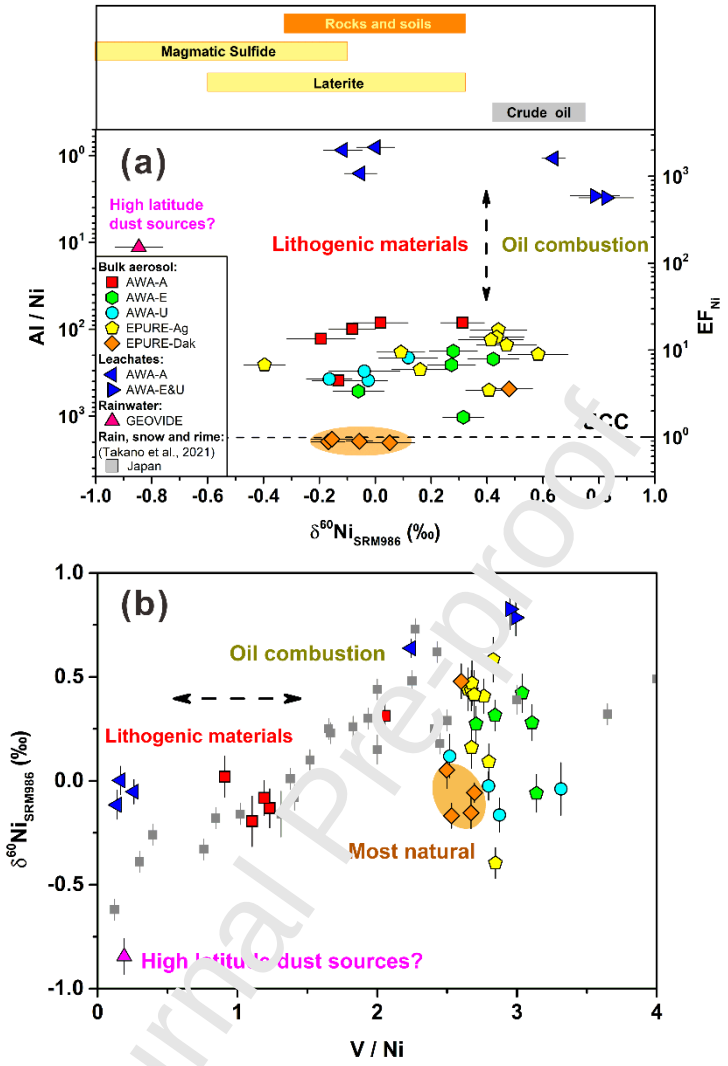

Figure 4. $\delta^{60}Ni_{SRM986}$ versus (a) Al/Ni ratios and (b) V/Ni ratios for aerosol, UHP water leachate and rainwater samples. Isotope compositions of different potential Ni aerosol sources are shown in the top part of (a) (rocks and soils from Gueguen et al., 2013; Estrade et al., 2015; Ratié et al., 2015, 2016, 2018; magmatic sulfide from Gueguen et al., 2013; Hofman et al., 2014; laterite from Ratié et al., 2015, 2018; crude oil from Ventura et al., 2015). Literature data for wet deposition from Japan (Mt. Kajigmori and Uji City) are shown in (b) (Takano et al., 2021). The dashed double-headed arrow in (a) represents the boundary of the crude-oil end-member, represented by $\delta^{60}Ni_{SRM986}$ higher than 0.4‰ (Ventura et al., 2015; Takano et al., 2020, 2021).

Figure 5:

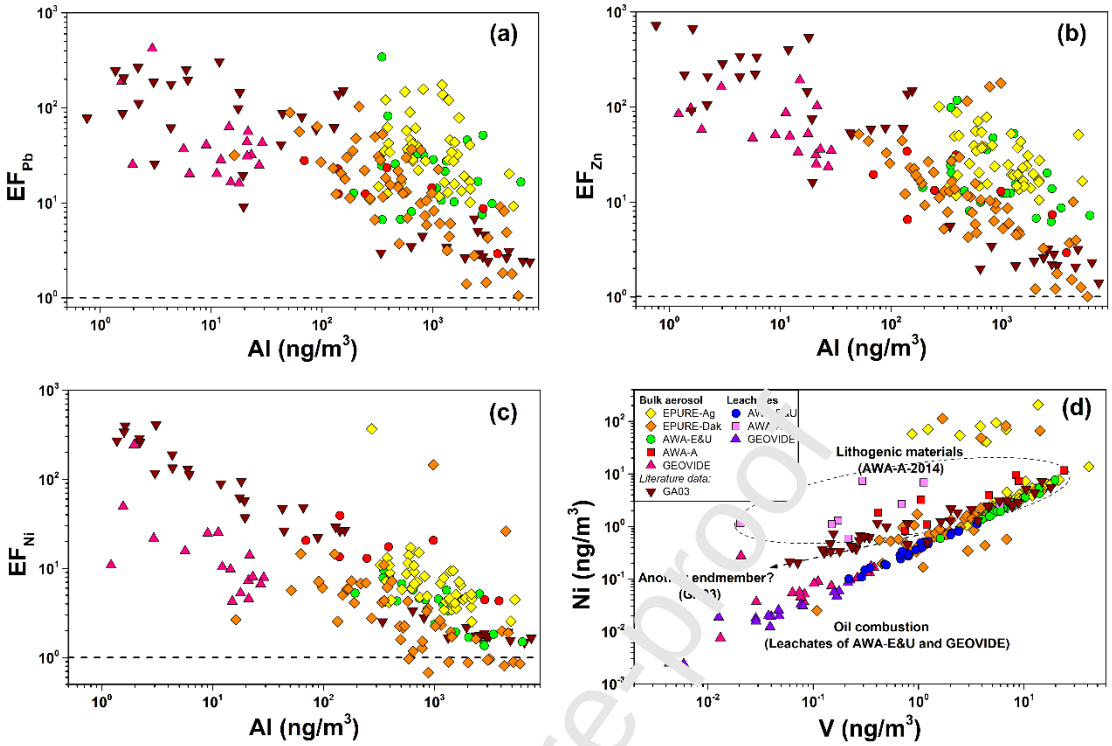

Figure 5. Correlations between atmospheric Al loadings and (a) EF_{Pb}, (b) EF_{Zn}, (c) EF_{Ni}, and between (d) Ni and V concentrations in aerosols. The elemental data for the samples from GEOVIDE, AWA and EPURE are from Shelley et al. (2016, 2017, 2018), those for the GA03 aerosols (US-GEOTRACES) from Shelley et al. (2015).

Figure 6:

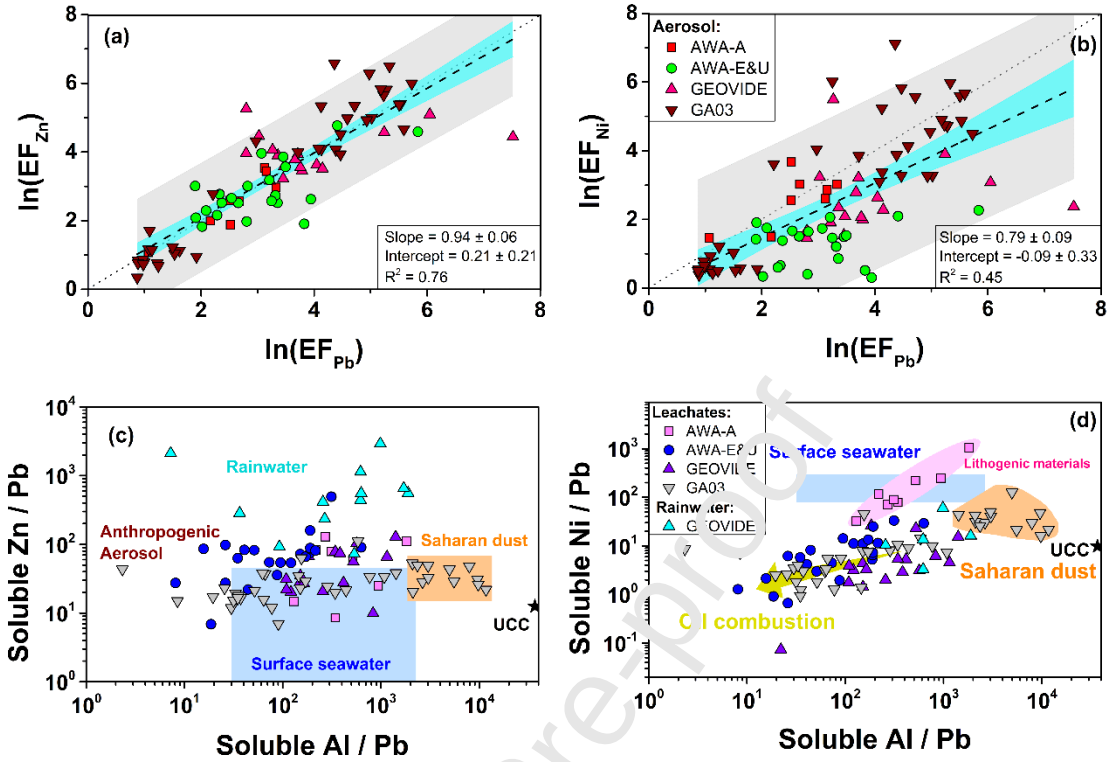

Figure 6. Comparisons of bulk aerosol enrichment factors (EF) between (a) Zn and Pb, and (b) Ni and Pb, as well as molar ratios for soluble (c) Zn/Pb and Al/Pb, and (d) Ni/Pb and Al/Pb. Bulk aerosol and leachate data for GA03 are from Shelley et al. (2015, 2018). The black dashed lines in (a) and (b) represent the least squares linear regressions. The light blue and grey areas indicate the 95% confidence and prediction intervals, respectively. The dotted lines represent the 1:1 line. The orange Sahara dust end-member in (c) and (d) is constrained by leachates significantly influenced by Saharan dust in Shelley et al. (2018). The large light blue rectangles in (c) and (d) show compositions of surface seawater in the North Atlantic (Conway and John, 2014; Hatta et al., 2015; Noble et al., 2015; Menzel Barraqueta et al., 2018; Zubrick et al., 2018; Lemaitre et al., 2020, 2022).

Figure 7:

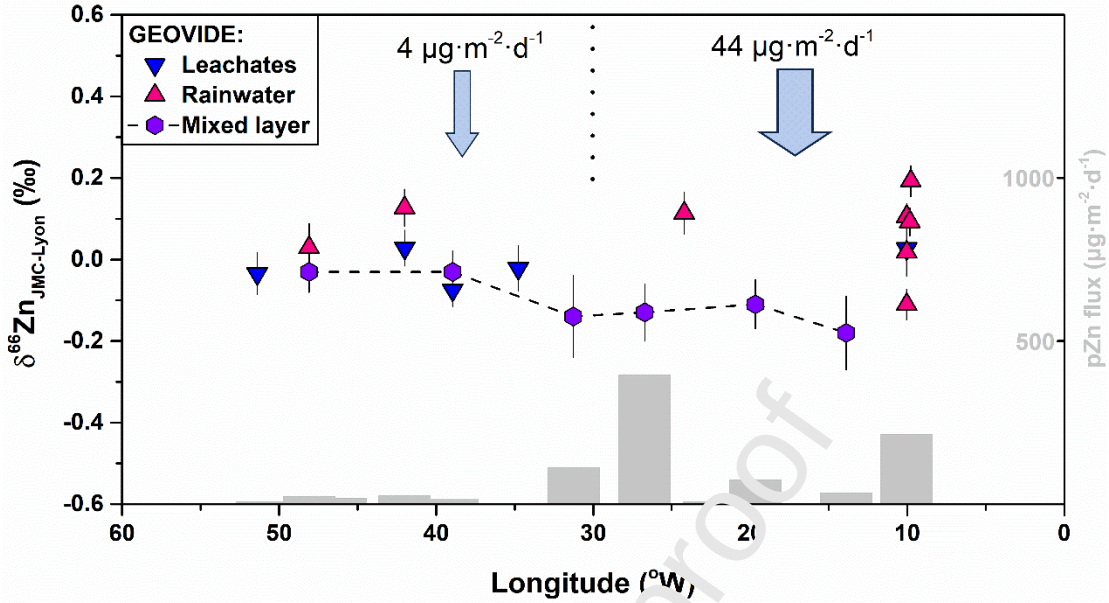

Figure 7. A comparison of $\delta^{66}Zn_{JMC\text{-}Lyon}$ between water leachates, rainwater and the surface ocean mixed layer for the GEOVIDE transect. The data for the mixed layer are from Lemaitre et al. (2020a). The dotted line near the top of the diagram indicates the boundary between the eastern and western sections (30°W), as defined by Shelley et al. (2017) for the calculation of atmospheric deposition fluxes. The light blue arrows represent the total soluble deposition fluxes from Shelley et al. (2017). The $_{P}Zn$ export fluxes at the equilibrium depth of ^{234}Th-^{238}U system are from Lemaitre et al. (2020b).

Figure 8:

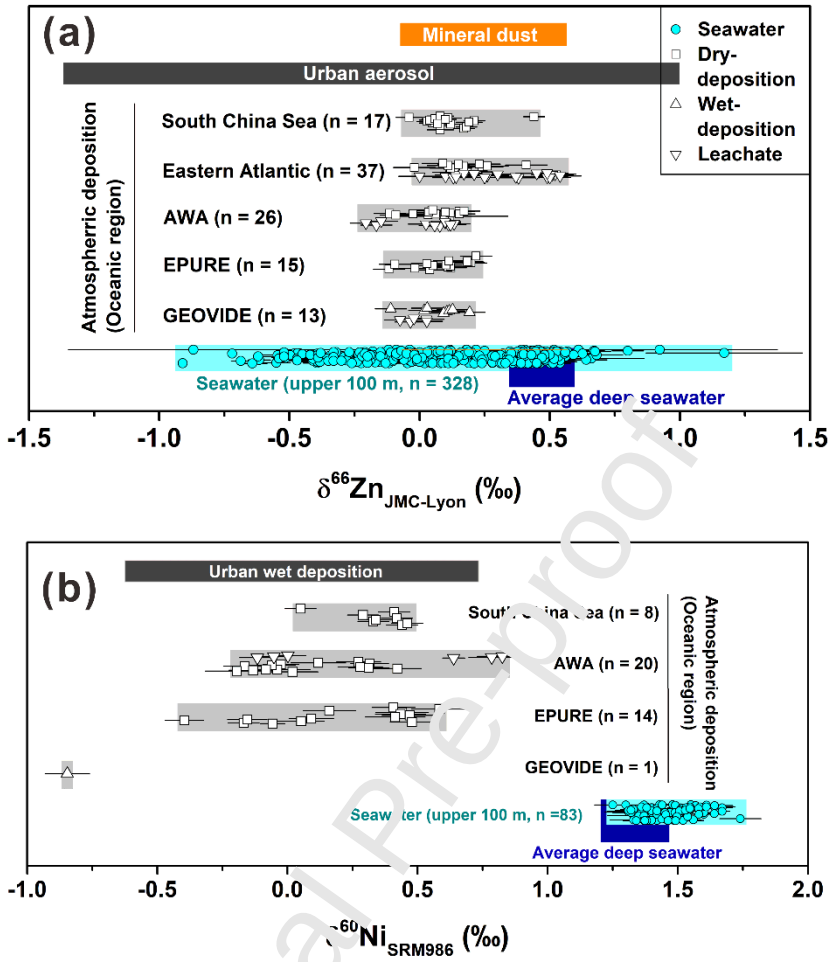

Figure 8. Measured isotope compositions of (a) Zn and (b) Ni for the oceanic regions studied here and in the literature (for Zn: Dong et al., 2013; Little et al., 2014; Liao et al., 2020, 2021; and for Ni: Takano et al., 2020, 2021) compared to data for mineral dust (in orange for Zn: Schleicher et al., 2020), urban aerosol (in black for Zn: Cloquet et al., 2006; Gonzalez et al., 2016; Dong et al., 2017; Souto-Oliveira et al., 2018, 2019; Schleicher et al., 2020; Jeong and Ra, 2021; Schleicher and Weiss, 2023) and surface ocean (in blue for Zn: Conway and John, 2014; Zhao et al., 2014; Conway and John, 2015; John et al., 2018; Vance et al., 2019; Wang et al., 2019; Liao et al., 2020; Lemaitre et al., 2020a; Sieber et al., 2020; and for Ni: Cameron et al., 2014; Takano et al., 2017; Wang et al., 2019; Archer et al., 2020; Yang et al., 2021; Lemaitre et al., 2022). The light blue bars show the range for the 100 m upper seawater isotope data, with the deep seawater average shown in dark blue.

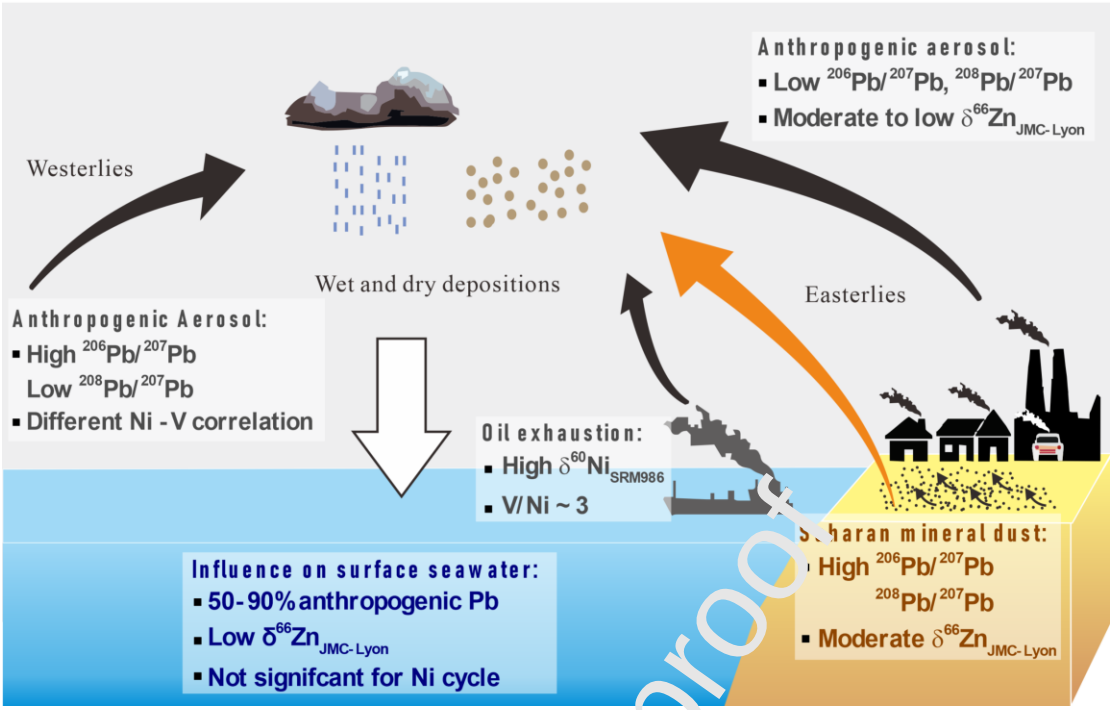

Highlights

- Impacts from Saharan dust, and high-T and low-T anthropogenic emissions can be identified with Zn-Pb isotopes;
- Nickel isotopes indicate contributions from oil combustion and lithogenic particles;
- The release of isotopically light Zn from anthropogenically sourced aerosol may be a key factor in determining the low $\delta^{66}Zn$ in surface seawater;
- These aerosols may be less significant for surface ocean Ni